INVESTIGATING GAIM-GM'S CAPABILITY TO SENSE IONOSPHERIC IRREGULARITIES VIA WALKER SATELLITE CONSTELLATIONS

THESIS

Brandon T. McClung, Captain, USAF

AFIT-ENP-MS-15-M-076

DEPARTMENT OF THE AIR FORCE
AIR UNIVERSITY

AIR FORCE INSTITUTE OF TECHNOLOGY

Wright-Patterson Air Force Base, Ohio

AFIT-ENP-MS-15-M-076

INVESTIGATING GAIM-GM'S CAPABILITY TO SENSE IONOSPHERIC IRREGULARITIES VIA WALKER SATELLITE CONSTELLATIONS

THESIS

Presented to the Faculty

Department of Engineering Physics

Graduate School of Engineering and Management

Air Force Institute of Technology

Air University

Air Education and Training Command

in Partial Fulfillment of the Requirements for the

Degree of Master of Science in Applied Physics

Brandon T. McClung, B.S.

Captain, USAF

March 2015

AFIT-ENP-MS-15-M-076

INVESTIGATING GAIM-GM'S CAPABILITY TO SENSE IONOSPHERIC IRREGULARITIES VIA WALKER SATELLITE CONSTELLATIONS

THESIS

Brandon T. McClung, B.S.
Captain, USAF

Committee Membership:

Dr. William F. Bailey
Chair

Dr. Stephen T. Fiorino
Member

Dr. Larry C. Gardner
Member

Dr. Robert D. Loper
Member

AFIT-ENP-MS-15-M-076

Abstract

GAIM-GM is a modularized physics based data assimilation model, that ingests data from multiple data sources. One data source is slant total electron content (TEC) from a ground station network to satellites, and along the occultation path between multiple satellites. This study examines GAIM-GM's capability to sense a scintillation feature in the ionosphere, overlaid on an IFM electron density grid, from simulated satellite constellations ingesting the slant TEC values into GAIM-GM. Satellite constellations were developed in an extension of MATLAB® called STK®. A real ground station network generated from IGS was ingested into STK® to compute access times to the satellite constellation and use the access data to compute the slant TEC values on the perturbed IFM grid. It was discovered that a Walker constellation would give the most frequent revisit time to the scintillation feature, which co-rotates with the Earth, capturing both the day and nightside ionosphere throughout the evaluation period (96 hrs). The size of the feature was varied along with the number of satellites in the Walker constellation. 25 different scenarios with these parameters varied were created to determine the sensitivity of GAIM-GM to sense the feature. A simple heuristic algorithm was applied comparing the truth data, in this case the perturbed IFM grid, to the GAIM-GM output in each scenario across the entire grid, and for those grid points within the feature.

Acknowledgements

First, I would like to thank my thesis committee chair, Dr. William Bailey. Dr. Bailey provided challenging and thought provoking ideas to help guide me through a long year of research. Dr. Bailey's tenure at AFIT proved very worthwhile, in engaging other departments within AFIT, and most importantly, the faculty at Utah State University, to allow for the completion of this research to be completed in a timely manner.

Next, I would like to highlight the importance of Dr. Larry Gardner, at Utah State University. His involvement in this research, was critical. Dr. Gardner spent countless hours adapting the GAIM-GM code to be able to ingest data files of the type generated, and provided pivotal feedback to ensure cross compatibility among the different platforms. With out his technical expertise, this research could not be completed. Additionally, I would like to thank Dr. Robert Schunk for allowing me to utilize Utah State University's facilities and equipment. The Air Force Institute of Technology looks forward to collaborating and continuing research with the Center for Atmospheric and Space Science in the future.

Additionally, I would like to thank my remaining committee members, Drs. Robert Loper and Stephen Fiorino. The feedback provided during the research process has been paramount, and allowed for the research to be taken to the next level.

Last, I would like to thank my fellow classmates and my family for providing support through the times of turmoil and a great social network. Cheers!

Brandon T. McClung

Table of Contents

Page

List of Figures

List of Tables

INVESTIGATING GAIM-GM'S CAPABILITY TO SENSE IONOSPHERIC IRREGULARITIES VIA WALKER SATELLITE CONSTELLATIONS

I. Introduction

1.1 Background

Ionospheric perturbations can cause a change in the phase and amplitude of a propagating electromagnetic plane wave while traversing a region of small scale irregularities in electron density. The resulting small scale changes in the index of refraction lead to differential diffractive scattering. This phenomenon is known as scintillation, and can degrade radio communications and the accuracy of global positioning systems. The results of this project will allow Air Force leaders to capitalize on degradation information, enhancing mission capabilities.

The faculty at the Utah State University developed an assimilation model, called the Global Assimilation of Ionospheric Measurement - Gauss Markov (GAIM-GM). This model feeds directly into the Air Force Space Weather forecast process, and provides decision makers with an accurate depiction of the current and future state of the ionosphere, and any potential mission impacts.

1.2 Problem Statement

To date, there have not been investigations on GAIM-GM's sensitivity to ingest data from different satellite constellations. GAIM-GM has the capability to ingest data from several sources, including observed total electron content (TEC) values

along a slant path from satellites communicating with a ground station network. The ability of GAIM-GM to ingest data of ionospheric perturbations, for different satellite constellations, and to accurately replicate an ionospheric irregularity is the subject of this research.

1.3 Research Objective

The objective of this research is to develop simulations, where different satellite constellations are created, and slant TEC observations made. The observations will be collected from a perturbed ionosphere characterized by modified Ionospheric Forecast Model (IFM) output, where an ionospheric irregularity will be manually placed in the IFM electron density output. These observations will be ingested into GAIM-GM, and a simple metric will be developed to determine GAIM-GM's capability to replicate the ionospheric irregularity.

1.4 Preview

This section will give a general outline of the remainder of this thesis. Chapter 2 will contain the literature review. It will start with a discussion of the basic properties of the Earth's magnetic field and its interaction with the ionosphere, along with the different types of irregularities that can occur in the ionosphere. The chapter will conclude with ionosphere modeling, touching on both the IFM and GAIM-GM. In Chapter 3, the methodology of the research will be outlined. Chapter 3 opens with a discussion on the modeling of the satellite constellations, followed by details of the numerical slant TEC calculation. The process of verifying this calculation with observed TOPEX data is discussed, proving ephemeris data can be used to make this observation. Then, the generation of the irregularities is discussed, concluding with all of the scenarios that will be examined, and how GAIM-GM's performance

will be measured. Chapter 4 will discuss the metrics used to determines GAIM-GM's capability to replicate the irregularities listed in Chapter 3. Trends in irregularity and satellite constellation size, will be discussed. Foremost, Chapter 5 will list the important conclusions discovered from this study, while opening up different channels of future research.

II. Background

2.1 Chapter Overview

This chapter provides the supporting information pertaining to the ingestion of slant TEC values into Global Assimilation of Ionospheric Measurements - Gauss Markov Model (GAIM-GM) from satellite constellations, to capture an ionospheric feature in the model's output. The chapter begins with an overview of the Earth's geomagnetic field, and properties of the ionosphere, followed by a discussion of ionospheric irregularities commonly known as plasma bubbles. The chapter concludes with information on ionospheric modeling, including discussions on the Ionospheric Forecast Model (IFM), GAIM-GM, and some of there validation studies.

2.2 Geomagnetic Field

Due to the rotation of the Earth and its metallic core, the Earth has a magnetic field that can be approximated as a dipole magnet, in the near-Earth environment or less than 6 Earth radii [10]. The Earth's magnetic field is responsible for dictating the movement of charged particles in the ionosphere. The dipole field is tilted by approximately 11 degrees from the rotation axis of the Earth [10]. As one moves poleward, the magnetic field lines become open and couple to the interplanetary magnetic field, and the solar wind. These open magnetic field lines allow energetic particles to enter the ionosphere, and can cause large density perturbations in the auroral regions during high solar activity [10].

The International Geomagnetic Reference Field (IGRF) is a model of the dipole-approximated magnetic field, using spherical harmonics. The IGRF obtains the expansion coefficients of the spherical harmonic components, by applying corrections from a global distribution of ground- and satellite-based magnetometer measurements

[13]. The IFM uses the IGRF to calculate the inclination, declination, and magnitude of the magnetic field, to aid in modeling the plasma physics within the ionosphere [1]. The next section will provide further information on the physics in the ionosphere.

2.3 The Ionosphere

The ionosphere is a region above the Earth's atmosphere, that contains free electrons, ions, and neutrals separating Earth's terrestrial atmosphere and interplanetary space [8] [13]. The physics of the ionosphere are different than that of the neutral, terrestrial atmosphere due to the free electrons and ions in the presence of the Earth's magnetic field, discussed in the previous section [8]. The photoionization process is the dominant process that drives the production of the ions and electrons. This process is dependent upon the neutral number density, $n(z)$.

$$n(z) = n_0 e^{-(z-z_0)/H} \tag{1}$$

Equation 1 provides the neutral number density, for a single species, as a function height, z, where n_0 is the number density at the reference altitude z_0. $H = kT/mg$ is the scale height, which is dependent upon the temperature and mass, m, of the individual species. The scale height H is also used to determine the optical depth, τ, of the ionosphere [13].

$$\tau = H\sigma_a n(z) \sec\chi \tag{2}$$

Equation 2 defines the optical depth for an idealized planar atmosphere, in terms of the absorption cross section, σ_a, which remains constant, the neutral number density, $n(z)$, defined in Equation 1, and χ, the solar zenith angle. Combining these functions with the ionization frequency, η, and the incident flux of radiation at the top of the

atmosphere, I_∞, yields the Chapman production function [13].

$$P_c(z,\chi) = I_\infty \eta \sigma_a n(z) e^{-\tau} \tag{3}$$

In general, the Chapman photoionization function, provided in Equation 3, describes the photoionization by the solar EUV and UV rays for a given number density profile. Using Equations 1 through 3 the vertical electron density profile for the ionosphere can be generated. Taking into account these chemical processes, the transport and diffusion of the ions and electrons in the Earth's magnetic field, several different layers are observed in the Earth's ionosphere. These regions are denoted as the D, E, and F regions. Sample vertical electron density profiles are portrayed in Figure 1.

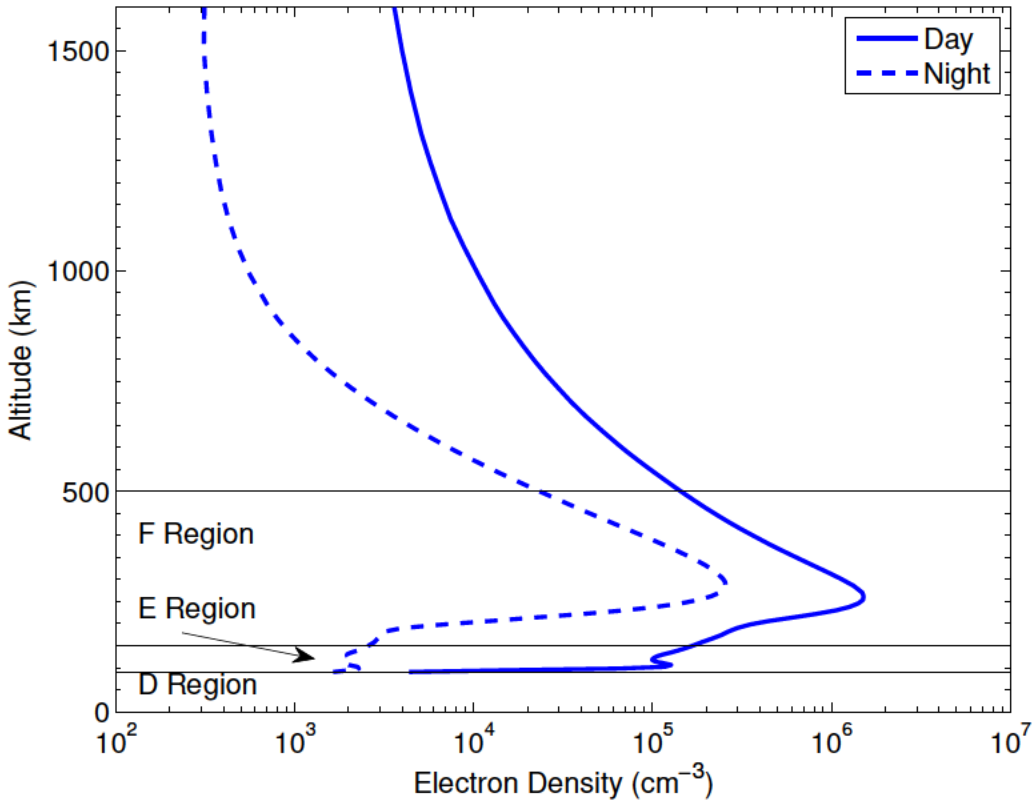

Figure 1. Day/night electron density profile for mid latitudes, derived from IFM electron density output for 2013/002/0015Z.

The vertical electron density profiles in Figure 1 are created from the IFM for the mid latitudes, both during day and night time on January 2, 2013 at 0015Z. There are two peaks associated with the electron density. The higher peak denotes the peak in the F region, where standard altitudes associated with the F region are 150 to 500 km, and major ion O^+. Below the peak in the F region peak is a second smaller peak, designating the E region [8]. In the F region, diffusion and transport need to be considered, whereas in the E region, chemical equilibrium can be assumed, and diffusion and transport can be neglected [13]. Standard characteristics of the E region include the major ions NO^+ and O_2^+, with an altitude starting near 90 km and extending upward to 150 km. Below 90 km is the D region where neutral number densities start to dominate, and become well mixed [8]. The day and night changes in the E and F region peaks are are directly related to the rate of photoionization. Once the sun is no longer providing the UV radiation, for ionization, the electrons quickly recombine with the major ions in the layer, thus reducing the electron density, as seen in Figure 1 [8]. The next section will discuss how the electric fields interact with a plasma density perturbation to generate plasma instabilities, leading to scintillation in the ionosphere.

2.4 Plasma Bubbles

Plasma bubbles are regions of depleted plasma density generated in the F region of the ionosphere, near the geomagnetic equator [8]. They were discovered with the use of a backscatter incoherent radar, in Jicamarca, located near the equator [13]. The regions of the depleted plasma caused noise in the radar signal, indicating a non uniform ionosphere near the equator. The plasma bubbles and depletions occur only at night when a strong plasma gradient exists on the bottom side of the F region due to the degradation of the D and E electron densities [8]. A schematic of the

requirements to allow a region of less dense plasma to accelerate upwards is provided in Figure 2.

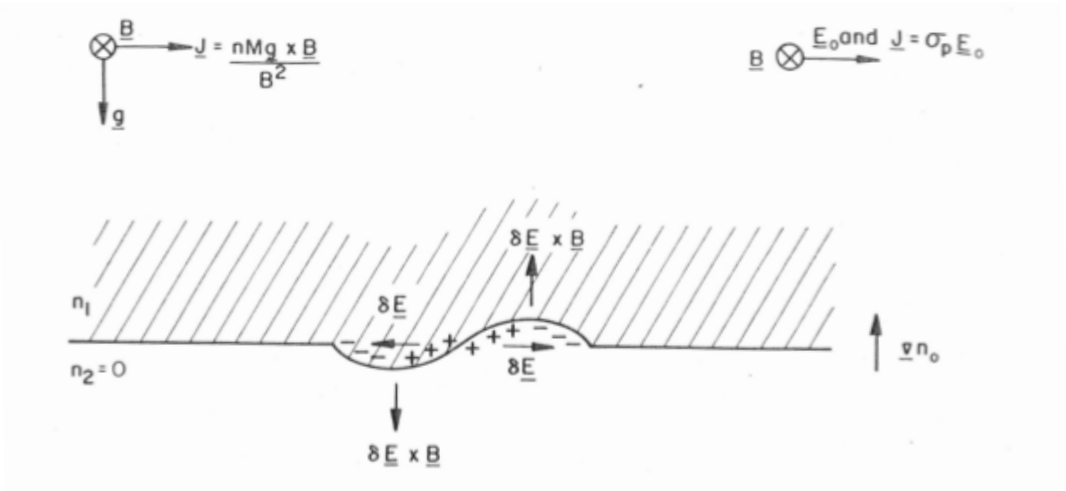

Figure 2. Diagram showing the physics driving the Rayleigh Taylor Instability. Adapted from Kelley, 1989, used with permission [8].

The perspective on this diagram is a vertical slice, at the equator, where north is directed into the page, south is directed out of the page, west is to the left, and east is to the right. The shaded region is a region of high density plasma, similar to that observed in the F region ionosphere, just after sunset, while the region below it is considered a low density, or D and E regions at night. Examining the schematic drawn in the upper left hand corner, it denotes that a current is derived as a result of the $\vec{g} \times \vec{B}$ drift velocity, from the gravitational force on the plasma in the shaded region. This current will allow for charge separation to occur in a perturbation region, resulting in a space charge electric field denoted as δE. This electric field interacts with the Earth's magnetic field, generating an upward drift velocity of the lower density plasma. This then accelerates the region of depleted plasma density upward. It has been observed that these plasma depletions can approach altitudes of 1000 km [13].

The result of these instabilities cause amplitude and phase scintillation. Amplitude scintillations can lead to signal fading, which can disrupt satellite communica-

tions or in the case of GPS severe phase scintillations can cause the GPS receivers to lose their phase lock, disabling some satellites in the GPS constellation [6].

Although in this research the physics of the Rayleigh Taylor instability on small perturbations will not be employed, a non-physical region of depleted electron density will be overlaid on an arbitrary 5 day period of IFM output. This modified IFM output will be considered the true ionosphere, and numerous satellite constellations will be flown above the true ionosphere sensing it via numerical slant TEC calculations on a real ground station network. These slant TEC measurements will then be ingested into GAIM-GM, and its output will be evaluated to determine its sensitivity and response to ingesting data from depleted regions in the ionosphere. The details of the depleted regions are presented in Chapter 3, along with details on the ground station network. The characteristics of IFM and GAIM-GM are discussed in the next section.

2.5 Modeling

As operations become more dependent on space, it is very important to capture the properties of the ionosphere discussed above in accurate models. The IFM and GAIM-GM model are two models used by operational Air Force personnel to aid them in characterizing the ionosphere.

2.5.1 Ionospheric Forecast Model

The IFM is a model of the global ionosphere that provides forecasts for molecular NO^+, O_2^+, O^+, and N_2^+ densities at E region altitudes, the two major and minor ions in the F region (O^+/NO^+ and N_2^+/O_2^+ respectively), proton and electron densities, and electron and ion temperatures globally from 90 to 1600 km. The model needs atmospheric densities and winds, magnetospheric and dynamo electric fields, auroral

energy fluxes with accompanying characteristic energies, in addition to a model of the geomagnetic field as inputs. These inputs are empirically driven, and self-contained within the model, where as the user-specified driver inputs are simple geophysical indices, including 3-hourly K_p and $F_{10.7}$ values [1].

The K_p index provides information on the average level of magnetic activity on a worldwide basis, by combining the K index, which measures the magnetic variability from the regular daily variation across three hours for 12 different observatories. The $F_{10.7}$ value is the value of the 10.7 cm wavelength flux received at the Earth, from the sun, which is a good indicator of solar activity [13].

Auxiliary outputs of IFM include the maximum electron number density in the E and F regions, N_mE and N_mF_2 respectively, and the heights that these density maximums occur in the E and F regions, h_mE and h_mF_2 respectively. Vertical TEC is an additional output variable, derived from the electron density grid. The TEC is a measure of the total number of electrons integrated between 90 to 1600 km over one square meter area, expressed in the TECu unit, where 1 TECu is the equivalent of 10^{16} electrons per square meter [1]. An example output is provided in Figure 3.

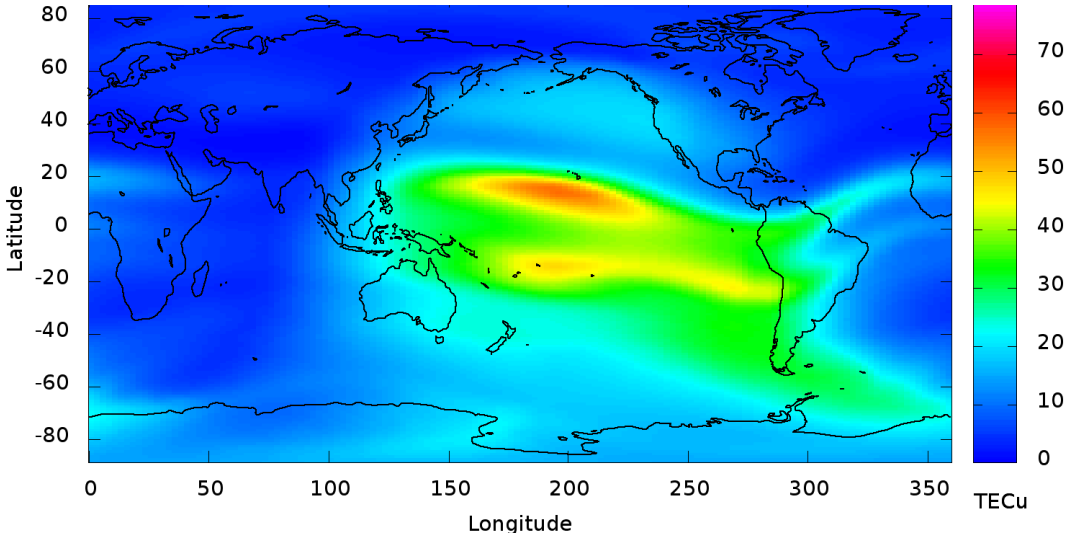

Figure 3. IFM total electron content (TEC) output, on 2013/001/0015Z.

The spatial resolution varies vertically, with a 4 km resolution in the E region altitudes and a 20 km resolution in the F region altitudes [14]. The zonal and meridional distributions are output on a geographic latitude and longitude grid, with a 3° latitude and 7.5° longitude resolution [1].

The inputs and drivers mentioned help provide a numerical solution to the ion and electron continuity, momentum, and energy equations. The physical processes encapsulated in these numerical calculations include field aligned diffusion, cross field electrodynamic drifts, ion production, thermosphere winds, neutral composition changes, thermal conduction, and elastic and inelastic heating and cooling processes. IFM also ensures the dominant physical process is weighted appropriately neglecting transport in the E region, and including transport for altitudes in the F region and above [1].

Output from the IFM will be utilized in two ways in this research. The plasma bubble like feature will be overlaid on every output file to represent a depleted electron density in the ionosphere. Additionally, the original output will be utilized by the Kalman filter in the GAIM-GM model, which is discussed in the next section.

2.5.2 Global Assimilation of Ionospheric Measurments - Gauss Markov

The GAIM-GM model is a physics based data assimilation model of the ionosphere, developed and ran at Utah State University. It uses the IFM as its background ionosphere. The model then uses ingested data to derive perturbations from the background state and uses the Kalman filter to assimilate the electron densities across the globe [15].

The schematic diagram in Figure 4 shows the various steps the model takes to assimilate the electron densities across the globe. After the user provides the inputs on the geophysical conditions for the physics based model, in Step 0, the physics based model is run in Step 1, including a data assimilation step, to allow for pattern

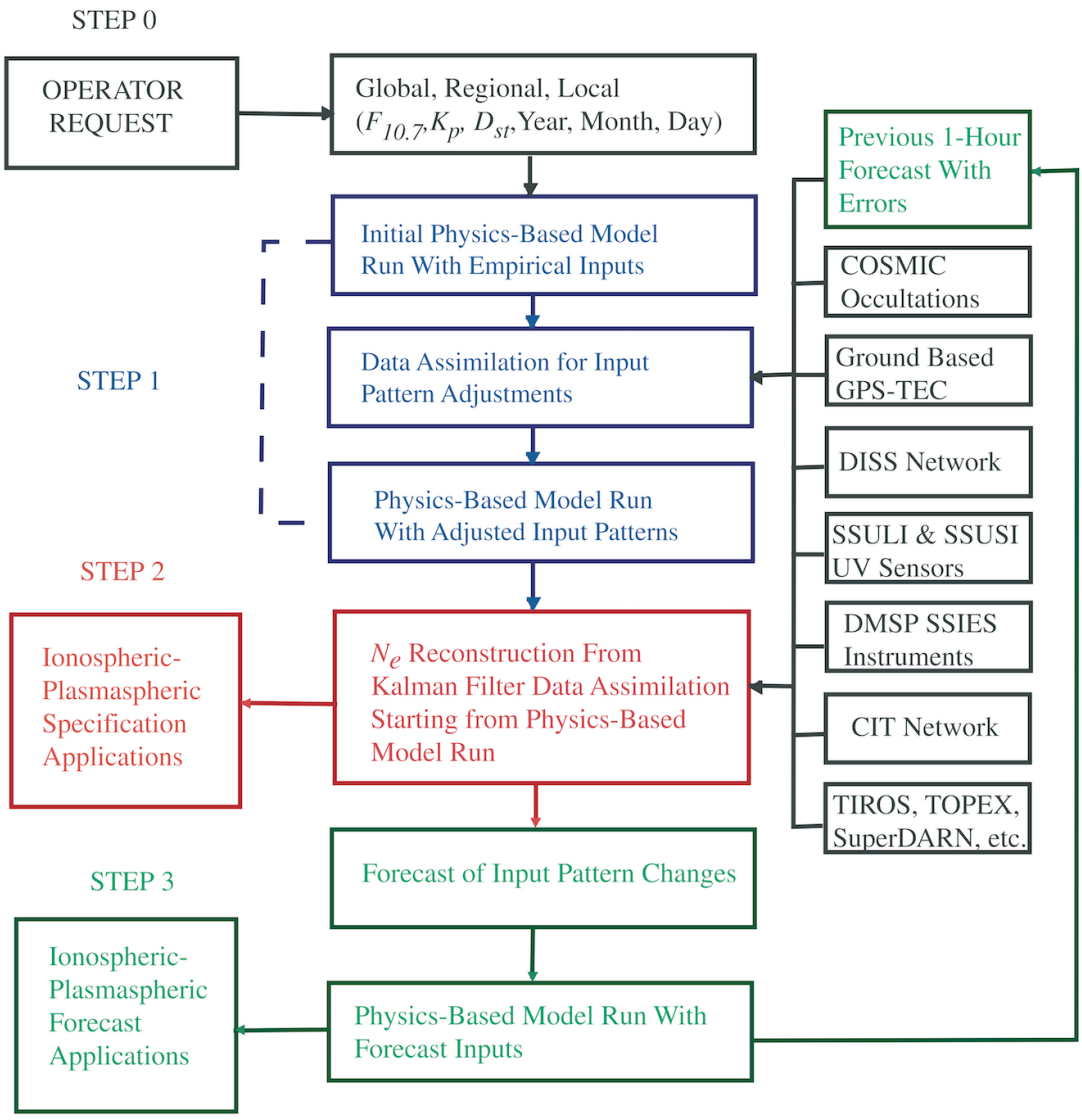

Figure 4. Schematic associated with a GAIM-GM model run. Adapted from Schunk 2004, used with permission [15].

adjustments, as indicated by the dark blue boxes. Of importance to this research is the right hand side black boxes, designating the inputs for data assimilation. In particular, this research will be simulating inputs in accordance with the ground based GPS TEC Measurements and Constellation Observing System for Meteorology, Ionosphere, and Climate (COSMIC) occultations, where instead of using the COSMIC satellite occultation different Walker Satellite constellations will be developed, and the occultation information between the satellites in the Walker constellation used in place of the COSMIC data [15]. The remaining inputs designated in the black boxes (DISS Network, SSULI and SSUSI UV Sensors, DMSP SSIES Instruments, CIT Network, and TIROS/TOPEX/SuperDARN) will not be utilized in this research, since the goal is to determine GAIM-GM's sensitivity to different satellite constellations, which is a control in this research.

The output resolution of GAIM-GM can be adjusted. There are 3 specified resolutions that are available, global, regional, and local. The local resolution needs to be used with caution, since in most cases the resolution of the input parameters is larger than the output resolution grid [15]. This research will use the output associated with the global mode. Output is generated in 15 minute increments, on a grid that extends from 92 km to 1380 km in altitude, with 4 km increments in the E region and 20 km increments in the F region. Zonally, there is a 4.667 degree latitudinal grid spacing and 15 degree longitudinal grid spacing. On this grid the primary output will be the electron number density distribution, accompanied with TEC in TECu units, N_mF_2, h_mF_2, N_mE, and h_mE, similar to the IFM [15]. The primary electron density distribution is generated using the Kalman filter, whose details are presented in the section below.

2.5.2.1 Gauss Markov Kalman Filter

The Kalman filter is a numerical method utilized to propagate information in time, while minimizing error [11]. The following section provides a description of the main equations used in the Kalman filter [7]. Equation 4 represents the model state vector $\mathbf{m}$, where the bold face represents a matrix.

$$\mathbf{m}^f = \mathbf{Lm} + \mathbf{b} \tag{4}$$

Equation 4 creates the temporal and forecast evolution of the model from its current state to the next forecast state, denoted by the superscript f. Within this equation is a transition matrix, $\mathbf{L}$, containing the dynamics of the model along with the transition model forecasting error, $\mathbf{b}$ [7]. Here the electron density perturbations will be contained in $\mathbf{m}$, with $\mathbf{L} = \mathbf{L_1 L_2}$, where $\mathbf{L_1}$ propagates the electron density perturbation state in time, and $\mathbf{L_2}$ contains a time constant that relaxes any perturbations in the electron density state, back to its background state [12]. The next step in the Kalman filter process is to compute the error covariance of the model, represented in Equation 5.

$$\mathbf{P}^f = \mathbf{LPL^T} + \mathbf{Q} \tag{5}$$

Equation 5 represents how the error covariance of the electron density perturbation is propagated to the next time step, with $\mathbf{Q}$ representing covariance in the model transition forecasting error, $\mathbf{b}$ [7]. Once the error covariance is computed for the forecast state, the observation state needs to be accounted for, which in this research will be the slant TEC values along the paths between the ground stations and satellites, shown in Equation 6.

$$\mathbf{d} = \mathbf{Gm} + \mathbf{n} \tag{6}$$

Equation 6 relates the current state, $\mathbf{m}$, or electron density perturbations, to a measurement matrix $\mathbf{G}$ containing the slant TEC observations, with $\mathbf{n}$ representing the observation error [7]. The role of equation 7 is to generate a matrix to incorporate the various model covariance errors and observations into the model final analysis state.

$$\mathbf{K} = \mathbf{P^f G^T}(\mathbf{GP^f G^T} + \mathbf{E})^{-1} \tag{7}$$

$\mathbf{K}$ provides the role of translating the observations from observation space to model forecast space, and is used to produce the final analysis state, in Equation 8..

$$\mathbf{m^a} = \mathbf{m}^f + \mathbf{K}(\mathbf{d} - \mathbf{Gm}^f) \tag{8}$$

Equation 8 represents the electron density perturbations adjusted for the TEC values observed by the satellites, in the next time step. This state is then used in 4 to then repeat the process and continue the Kalman filter process for the desired amount of time steps [7]. The last step in the Kalman filter process is to compute the model error covariance matrix for the new forecasted state, shown in Equation 9.

$$\mathbf{P^a} = (\mathbf{I} - \mathbf{R})\mathbf{P^f} \tag{9}$$

The results of this research depends on how the Gauss Markov Kalman filter handles the perturbation densities ingested into GAIM-GM, from the satellite constellation created. The perturbation density will be implemented in the form of a depleted electron density region, and the constellation will be designed to ensure the slant TEC calculation penetrates the plasma bubble. The details of these calcula-

tions, the constellation, and the implementation of the depleted region on the IFM grid, are discussed in the next chapter.

2.5.3 Model Validation

Validation studies are an important way to verify that the numerical model employed is accurately performing the calculations. Verification studies have been performed on both the IFM and GAIM-GM models, using data from the Ocean Topography Experiment (TOPEX) and Poseidon satellite.

In verifying the IFM output, TEC data from the TOPEX study was used to validate the model. Poseidon's mission was to study sea surface height anomalies over the ocean [19]. The satellite measures the sea surface height, by using a dual frequency radar altimeter. The altimeter operates at frequencies of 5.3 and 13.6 GHz. A dual frequency altimeter is required to minimize scintillation errors due to the plasma in the ionosphere. Since the ionospheric plasma disperses radar waves emitted by the altimeter, a TEC value can be derived from the difference in phase of the reflected waves off of the ocean surface [3]. The orbital mechanics of the satellite allow for nearly global coverage of the oceans, enabling TOPEX to be a good dataset for validation of the global TEC values for the IFM grid [19]. The validation study was performed over a number of geophysical conditions, and the results of the TOPEX measurements were binned by season, solar activity, and geomagnetic activity [19]. The results proved that the IFM TEC distributions were consistent with the TEC distributions of the TOPEX data. This study motivated an investigation of the numerical slant TEC function adopted from Utah State University, and outlined in the methodology. With TEC data available via file transfer protocol on NASA's website, a validation study of the slant TEC calculation was performed. Details and results of this verification are discussed in the next chapter.

TOPEX data was also used to provide a validation of the GAIM-GM electron density profiles. A 30 day study was conducted, for varying configurations of data ingested into GAIM-GM, including slant TEC values from the TOPEX satellite to the ocean surface. The study again, was conducted over the oceans, and determined that GAIM-GM produced TEC values closer to the observed TOPEX TEC values when the slant TEC values observed from the TOPEX satellite were ingested into GAIM-GM [16]. This is an important result for the research presented because a global ground station grid is being used, which will allow for slant TEC values to be ingested over land. With the ingested TOPEX slant TEC data providing a better result, it is indicative that ingesting slant TEC data over land will also improve the GAIM-GM output.

III. Methodology

3.1 Chapter Overview

This chapter outlines the steps taken to build the files ingested by GAIM-GM. This chapter provides information on how the satellite constellations were modeled, the slant TEC calculation was performed, and how the feature was created on the IFM electron density grid. With this understanding, it should be easy to see how the calculations from the satellite constellations on the modified electron density grid created an ingest file for GAIM-GM. The chapter then describes a simple validation study using TOPEX data, and the numerical slant TEC calculation, and provides a list of the feature sizes and constellation combinations. The chapter ends with a discussion on how the GAIM-GM output was evaluated, to determine how well GAIM-GM was able to recreate the feature.

3.2 Satellite Constellation

This section will discuss the orbital mechanics of the satellite constellations implemented in each scenario. In detail, the design of each satellite will be discussed, a discussion of a Walker constellation will follow yielding to a discussion of the way these constellations were simulated in the STK® environment.

3.2.1 Satellite Design

A few assumptions need to be made on the satellites that were used in this analysis. In reference to Nava's work [9], it is important to state that the payload's on the satellites were identical to those of a standard GPS satellite, allowing for the slant TEC values to be calculated. However, due to the numerical nature of this calculation discussed later in this chapter, the payloads do not need to be simulated in

STK®. The next section will discuss how these satellites are used to create a Walker constellation.

3.2.2 Walker Constellations

Walker constellations are a very common satellite constellation. The GPS satellite constellation is a great example of a Walker constellation, where multiple orbital planes exist in the constellation with numerous satellites in each plane. This constellation is considered to have a circular orbit, maintaining a constant altitude as it orbits the Earth. The 4 key parameters that play into the design of any satellite constellation are the inclination angle, the total number of satellites in the constellation, the number of planes and the spacing between the satellites in the different planes.

In this analysis, the inclination angle, or the north-south latitudinal extent, remained constant at a value of 50 degrees. The ionospheric feature was centered on the equator, hence sensing the high latitude ionosphere was not of interest. The total number of satellites in this analysis was increased throughout the analysis, as was the number of planes in the walker constellation. The number of planes in the constellation was the same as the number of satellites in the constellation, yielding one satellite per plane. The right ascending ascension node (RAAN) of each satellite in the constellation was spaced evenly across the globe, starting from the 260 degree meridian (STK® default). For example, in a 4 satellite constellation, the starting point of each satellite was at at 80, 170, 260, and 350 degree longitude at the equator. The orbit of each satellite was circular at an orbit altitude of 2000 km allowing for the entire modified electron density grid to be characterized by the constellations.

The Walker constellation was chosen so that the revisit frequency to the feature in the ionosphere will be maximized [17]. Other satellite constellations were discussed, but it was determined that the revisit frequency to the feature of interest would not

be maximized. Maximizing the revisit frequency is important, so the Kalman filter in the GAIM-GM model ingests the irregularity data more frequently, and propagates that forward in time. The next section will describe how these constellations were developed in an extension of MATLAB® known as STK®.

3.2.3 Systems Toolkit Software, STK®

Systems Toolkit, developed by Analytical Graphics Incorporated, is a physics based software geometry engine that accurately displays and analyzes land, sea, air, space assets in real or simulated time [18]. The software has two programming interfaces that can be used in conjunction with MATLAB® coding practices. The first is MexConnect which parses together a string command, then feeds it into an execution engine and displays the command on the STK® graphical user interface (GUI). The second option is using the object model, which provides access to object oriented programming constructs, in this case C♯, and allows the programmer to modify the scenario in STK® and extract object properties within the scenario [18]. This research used the object model construct to allow easy access to the different properties of the satellite and ground station network.

For each combination of constellation and feature size, a new STK® scenario was created. The scenario was created with a start and end time and a time step that can be referenced later when extracting various properties of the satellites. The length of time the analysis took was dependent upon the time step due to the write time of each of the data points. For each scenario, a time step of 1 minute was used. Once the STK® scenario was created, a real GPS ground station grid was loaded into the scenario. The grid used was the International Global Navigation Satellite System Ground Station Network (IGS) shown in Figure 5. Each ground station location is represented by a circle on the map. The latitude and longitude boundaries of the

features to be analyzed are also shown.

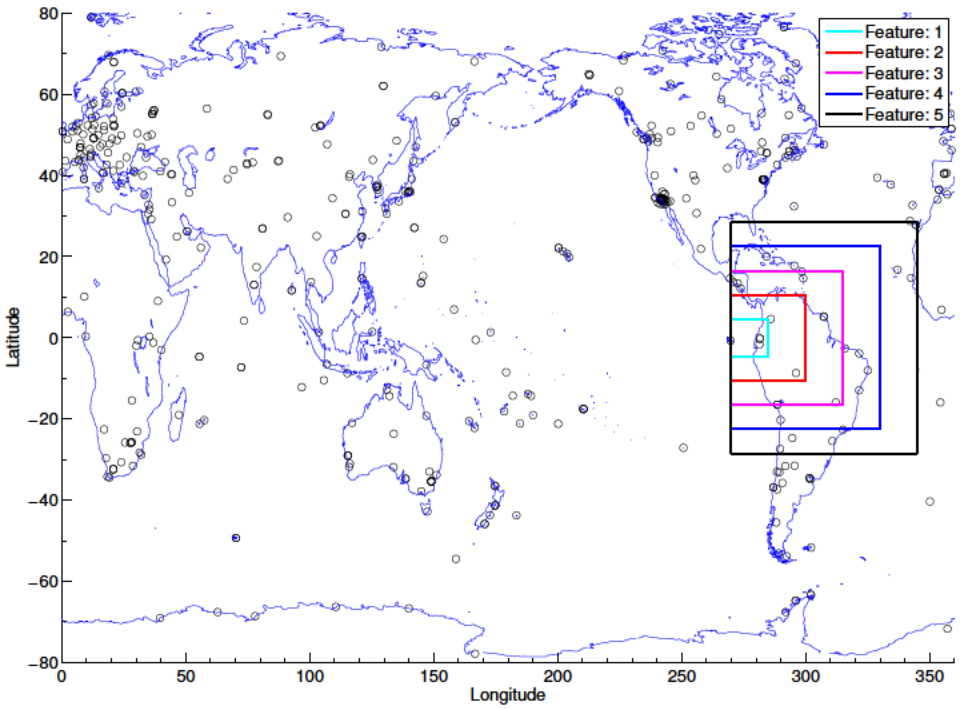

Figure 5. The IGS grid with the latitude and longitude boundaries of the 5 different features.

The geodetic latitude, longitude, and altitude information of 453 ground stations across the globe was downloaded from http://igscb.jbl.nasa.gov, and used to create facility objects in STK® [5]. Once this ground station grid was loaded, the satellite constellation was created using the object model time step and start and end times. In the cases where multiple satellites are in the constellation, the RAAN was adjusted to ensure the satellites were in different planes. A 3-D example showing a 9 satellite constellation modeled in STK®, is shown in Figure 6.

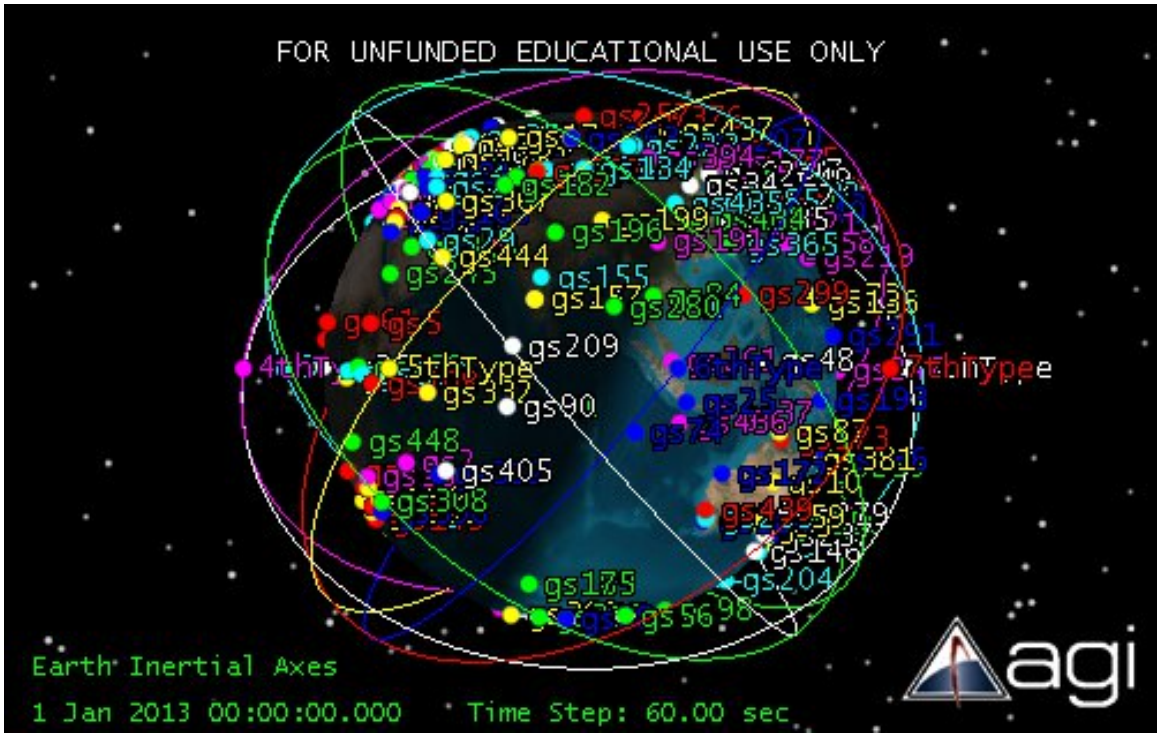

Figure 6. 9 Satellite Constellation, modeled in STK®.

STK® has the capability to compute when the satellites are visible to the ground station grid and to other satellites; termed Access data. The Access data is an object property that can be generated between two objects in STK®, in this case the Access data was generated between each satellite and ground station pair, and when the satellites in the constellation could see each other over the entire simulation period. A visualization of the Access data is presented in Figure 6 for one ground station, and 9 satellites in the constellation. The teal lines indicate the ground track of the satellites, when the satellite was visible to the ground station for the simulation window.

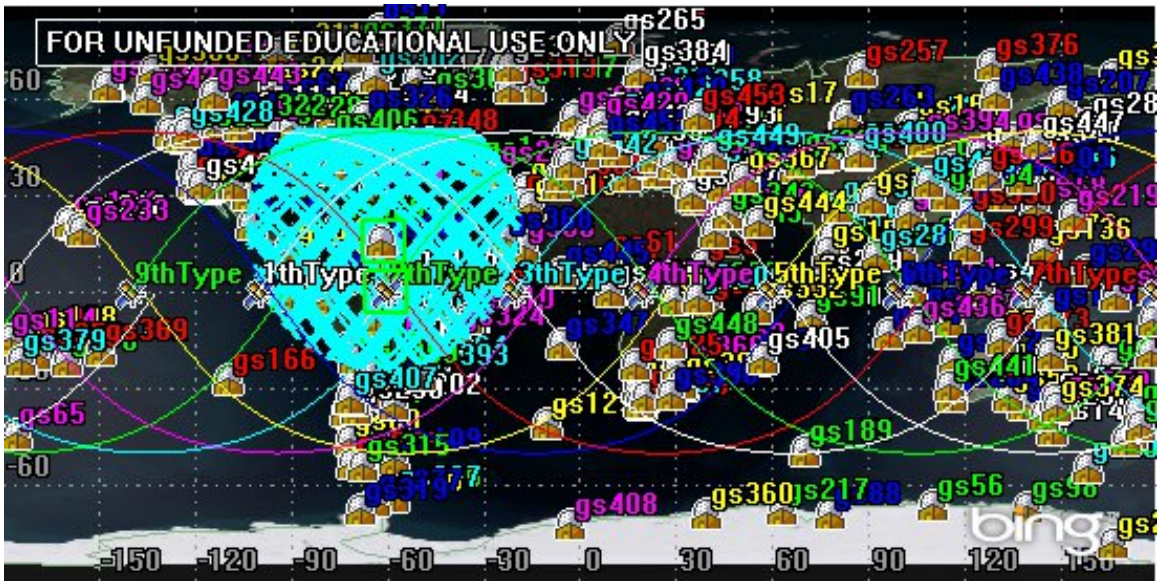

Figure 7. Access data visualization for 1 ground station, and 9 satellite constellation.

STK® allows the user to specify restrictions on when the satellite has access to other objects. The restrictions can only be applied when both the satellites and ground stations have transmitters and receivers loaded onto each. It was determined that adding these features would not increase the data points ingested thus the implementation of these features was deemed unnecessary. The default Access properties in STK® were used, which implies that once the satellite was visible over the horizon to the ground station (even with an elevation angle of zero) the satellite was considered to have access to the ground station. In contrast with Nava's research where an elevation angle mask was applied, a similar technique was not applied here because GAIM-GM has the elevation angle mask included in its data ingestion scheme, and rejected data points with elevation angles less than 15 degrees [9].

The latitude, longitude, and altitude information for the satellites contained in the Access data was exported to a .mat file in MATLAB® to allow for accessibility across multiple computing platforms (i.e. Windows and OSX). This data was then used to compute the slant TEC values to be ingested into GAIM-GM. Details on how

the Access data was transformed to build the GPS and satellite occultation ingest files is provided in Appendix A. The next section provides details on how the slant TEC calculation was made.

3.3 Slant TEC Calculations

Using the electron density values on the modified or background IFM grid, a numerical solution was obtained for the total electron content (TEC) between two points, in TECu units. Nava adapted this method into MATLAB® from the Utah State University's FORTRAN code [9]. In this study, two slant TEC values were ingested into GAIM-GM. One calculated from the satellite to the ground station, and from one satellite to another. However, when the calculation was made on the modified IFM electron density grid, the occultation path between two satellites never intercepted the feature due to the high orbital altitude of the satellites.

The inputs required to make the slant TEC value were the latitude, longitude, and altitude of both the ground station or satellite and another satellite. Additionally, it requires the appropriate IFM electron density grid for the appropriate time. The correct IFM file was loaded depending on the time given by the STK® Access data. With this information, the function converted the latitude, longitude, and altitude information into an Earth-Centered-Earth-Fixed (ECEF) reference frame, where the vector between the ECEF coordinates of the GPS ground station or satellite and another satellite was computed. The length of this vector was computed, then a bin size was determined by dividing the length of the difference vector by the average IFM vertical grid resolution, 5 km. Once the difference vector, or path, was binned up, the electron density was computed along the path at each bin. This was done using a weighting technique called the parametric approximation. It determined the electron densities at the nearest 8 IFM grid points, then weighted these values appropriately

to determine the electron density at the binned location. Once the electron densities were known for all binned locations, they were numerically integrated, and converted to total electron content units (TECu). This algorithm was verified using pre-existing TOPEX data and this result is discussed in the next section.

3.4 TOPEX Validation Study

As discussed in section 2.5.3, TOPEX is a satellite, equipped with a radar altimeter, used to measure sea surface height anomalies. Due to the dual frequency nature of this altimeter a TEC value can be calculated from the signal reflected off of the ocean surface. This simple verification examined three passes over the open ocean during weak geophysical conditions. The intent of this analysis was to test the accuracy of the numerical slant TEC calculation method, and show that using latitude, longitude, and altitude data from an existing satellite, that an accurate slant TEC calculation could be computed on a model grid.

The time period examined during this study covers 48 hours from 005/1996 through 007/1996. For this time period, IFM output was generated and downloaded from Utah State University. Additionally, TEC and ephemeris data from TOPEX for three passes was obtained via file transfer protocol. IDL, a simple scripting language, was used to read the ephemeris and TEC data from the binary file type and export it into a text file. Once exported into a text file, the text file was read into MATLAB®, storing the ephemeris data and temporal information. From the temporal information provided in the binary TOPEX data, the correct IFM file was determined, opened using netcdf. Using the latitude, longitude, and altitude information, the TEC was computed from the satellite's position to the sea surface on the corresponding IFM electron density grid. This was done for all ephemeris points for the three passes. These values were then compared to the observed TEC readings. The

satellite ground tracks for the three different TOPEX passes examined are shown in Figure 8.

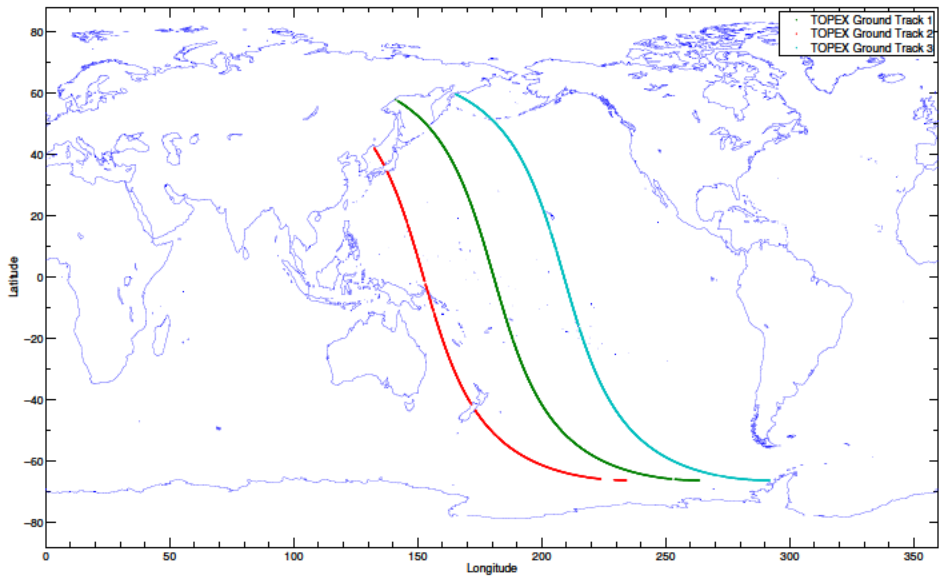

Figure 8. Ground tracks of the 3 TOPEX passes examined.

It is important to note that the TEC could only be calculated over the water, due to the radar altimeter on the satellite. That is why in Figure 8 there were no ground track data available over the Japan and some Pacific Islands. The observed TOPEX TEC values are presented along with the numerically derived TEC values at each ephemeris point in Figure 9.

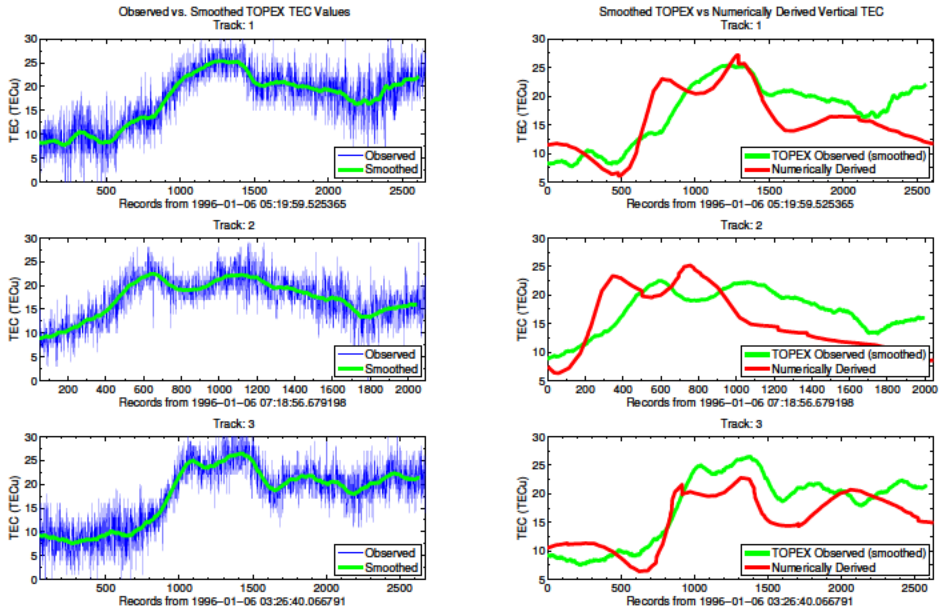

Figure 9. Smoothed TEC values vs. observed TEC values (left), smoothed TEC values vs. numerical TEC values (right), for 3 TOPEX passes.

The plots on the left hand side of Figure 9 are noisy due to the bias of the radar altimeter. In order to get a clean comparison to the numerically calculated slant TEC values, a smoothing algorithm was applied to the data. For each data point, an average of the previous and next 50 points was calculated and assigned to that specific point. This was then completed for all points of the data to yield the green line, in the left column, of Figure 9.

Figure 9 also shows the smoothed TEC values from TOPEX overlaid on the numerically calculated TEC value on the IFM electron density grid, on the right hand side. It is seen that the numerically calculated TEC values fall within the bias of four TECu, previously determined at Utah State University [19]. This proves that the algorithm to compute TEC on the electron density grid is valid and can be used to compute slant TEC values along the path between the ground station and satellites, or the occultation path between the satellites. The next section details how the

scintillation feature was overlaid on the original IFM electron density grid.

3.5 Scintillation Feature

It was shown in Chapter 2, that plasma bubbles are regions of depleted density in the night time ionosphere, that cause scintillation. Since the IFM model physics is not designed to handle the development of plasma bubbles in the equatorial region, the bubbles have to be placed on the electron density grid manually. Nava developed an accurate method to do so, where the plasma bubbles co-rotated with the Earth and were aligned along the Earth's geomagnetic equator [9]. Nava's method was analyzed under the research of Fenton, who investigated GAIM-GM's capability to handle the plasma bubbles without additional inputs. Fenton determined that GAIM-GM handled the evolution of the plasma bubbles poorly [2]. With the results of these previous researchers, it was determined that in this study applying the physics of the plasma bubbles was not needed. Instead, the capability of GAIM-GM to re-create a non-physical feature overlaid on the IFM electron density grid was examined.

In this research, a simple square box, in a latitude and longitude projection, was implemented as the scintillation feature overlaid on the IFM electron density grid. The box was centered latitudinally over the equator with the westward extent fixed on the 270 degree longitude. Within the feature, the electron density values on the IFM grid points were set to zero. The size of the feature was varied to assess GAIM-GM's ability to sense and replicate. The properties of the five scintillation features used in this research are provided in Table 1.

Table 1. Feature Number and Sizes Analyzed

Feature #	N-S Extent	W-E Extent	Vertical Extent
1	9° / 990 km	15° / 1650 km	104 km
2	21° / 2310 km	30° / 3300 km	200 km
3	33° / 3630 km	45° / 4950 km	306 km
4	45° / 4950 km	60° / 6600 km	408 km
5	57° / 6270 km	75° / 8250 km	504 km

The feature size was fixed to nodes on the IFM grid, rather than distance, thus negating the necessity for interpolations of electron density values on the IFM grid. There was no transitional smoothing implemented, meaning one grid point outside of the box had the background IFM electron density value, while the next grid point determined to be within the feature had an electron density value of zero.

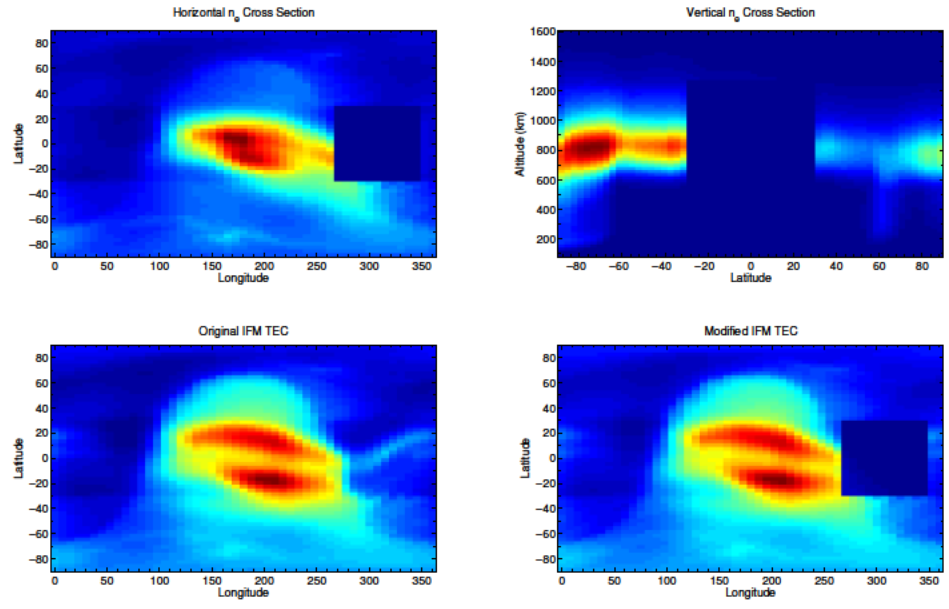

Figure 10. Top: Feature 5 overlaid on IFM electron density grid, horizontal (left) and vertical (right). Bottom: Background (left) and modified (right) TEC values for Feature 5.

The vertical and horizontal cross sections of the largest feature analyzed, Feature 5 in Table 1, are shown in Figure 10 in the top row. The bottom row shows the background IFM TEC values on the left, then on the right the modified TEC values are seen. The modified TEC values were obtained by using the slant TEC calculation at each latitude and longitude grid point within the feature for altitudes just above and below the model boundaries. This ensured that the TEC calculation, captured the electron densities above and below the feature. The next section provides the various combinations of the feature size and satellite constellations to be analyzed.

3.6 Size and Constellation Combinations

In total, 25 different scenarios were examined. Table 2 shows the 5 different sized features and the Walker constellations used to examine that particular feature. Each plane in the walker constellation had one satellite. The planes were distributed evenly across the globe to ensure maximum coverage. The orbital period of each satellite was 132 minutes, with 11 revolutions per day. A 60 second time step was used, meaning for each Access interval (on average 10 minutes) a slant TEC calculation would be made every 60 seconds, yielding 10 inputs for that particular Access interval.

Table 2. Feature Number and Walker Constellations Analyzed

Feature #	Number of Satellites
1	$1, 3, 5, 7, 9$
2	$1, 3, 5, 7, 9$
3	$1, 3, 5, 7, 9$
4	$1, 3, 5, 7, 9$
5	$1, 3, 5, 7, 9$

Ingest files were generated for all 25 scenarios portrayed in Table 2. Once the files were created, they were uploaded to the GAIM-GM server at Utah State University. Once they were uploaded, the GAIM-GM executable files were reconfigured to ingest the files for each scenario and GAIM-GM was run [4]. Once each run was complete

the GAIM-GM output files were downloaded to a local machine and the data were evaluated using two simple metrics outlined in the next section.

3.7 Evaluation

Using the TEC output from both the GAIM-GM and IFM grids, metrics were developed to evaluate GAIM-GM's capability to re-create the scintillation features, that were inserted into the background IFM electron density grid. These metrics were evaluated spatially and temporally, across the 96-hour forecast window, including the 24-hour warm up period for GAIM-GM. There were two different evaluations completed. The first type titled global evaluation looked at the entire GAIM-GM grid across the globe, where the data ingested was from the modified electron density grid. The second type of evaluation examined the times when only the path between the satellite and ground station intercepted the scintillation feature. This is termed local evaluation. The details of these evaluations are provided in the sections below, along with how the IFM and GAIM-GM grids were mapped to the same grid size for analysis.

3.7.1 Interpolation Scheme between IFM and GAIM-GM Grids

This section provides information on the IFM and GAIM-GM model grids. Specifics on how data from the IFM grids was interpolated to the GAIM-GM grid for evaluation are also provided.

The latitude and longitude grid points of the GAIM-GM grid are shown in Figure 11. The GAIM-GM grid is non-uniform, with the latitude increment between grid points in the mid-latitudes being 4.667 degrees and in the polar regions the latitudinal resolution increases in coverage, with the grid point spacing at 3 degrees. GAIM-GM has a longitudinal grid spacing of 15 degrees.

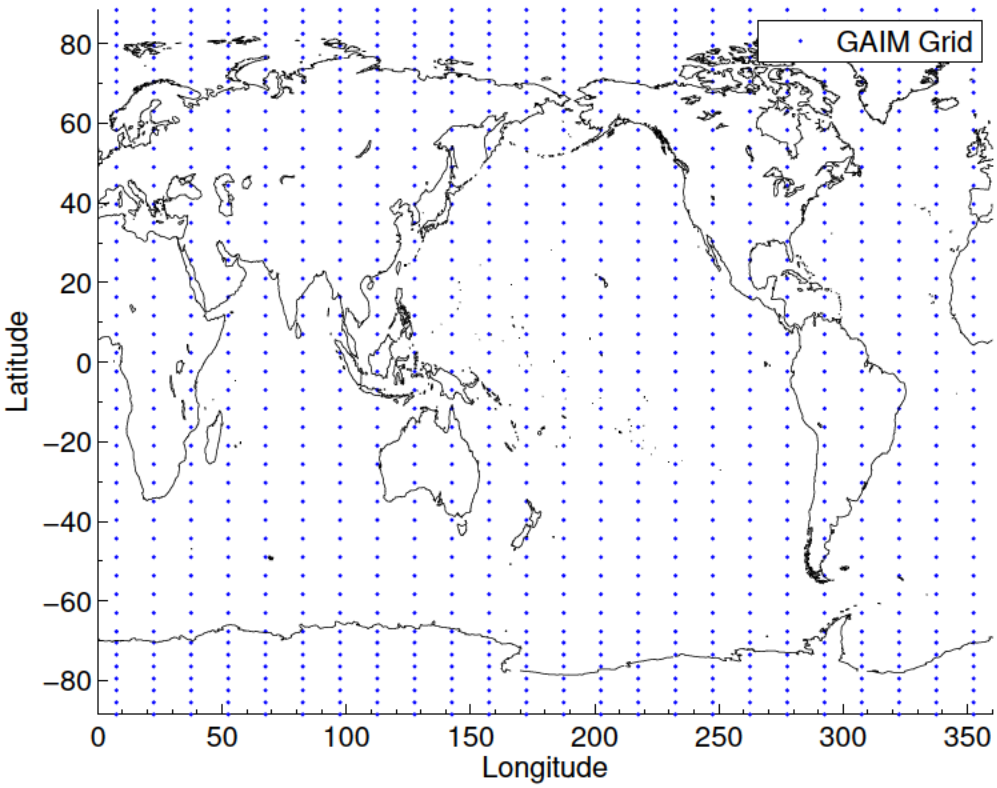

Figure 11. The blue dots represent the latitude and longitude grid points for the GAIM-GM output.

The latitude and longitude grid points of the IFM grid point are shown in Figure 12. It is seen that this grid is uniform across the globe, with latitudinal spacing at 3 degrees and longitudinal spacing at 7.5 degrees. Thus the GAIM-GM and IFM grids are not coincident.

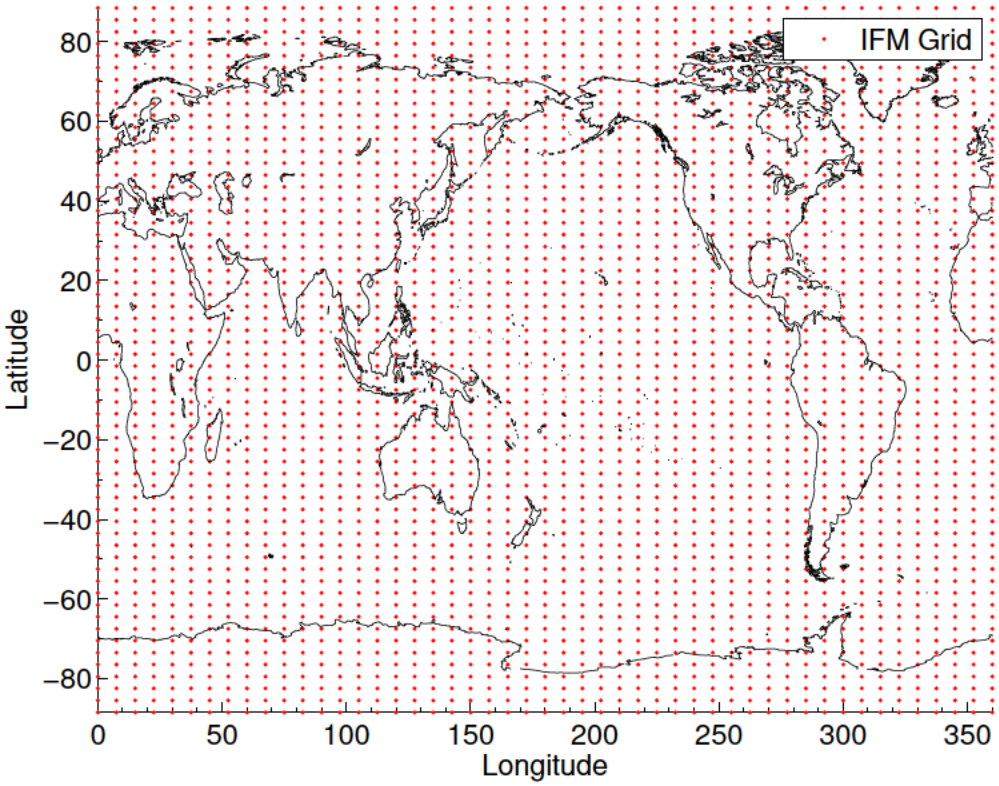

Figure 12. The red dots represent the latitude and longitude grid points for the IFM grid.

In order to assess GAIM-GM's ability to sense and replicate scintillation features, the modified IFM TEC input values had to be interpolated via a nearest neighbor interpolation scheme from the IFM grid to the GAIM-GM grid. When done, TEC value comparison metrics are used to measure success. The metrics used to quantify GAIM-GM's sensitivity to the different satellite inputs are presented next.

3.7.2 Metrics

Two different metrics were developed to help determine how well GAIM-GM was able to replicate the scintillation feature overlaid on the IFM electron density grid. They are the ratio metric and the difference metric, whose definitions, equations, and

ideal values are outlined below.

3.7.2.1 Ratio Metric: R

The ratio metric is defined in Equation 10. It is referred to as the ratio metric, since it measures directly the ratio between the GAIM-GM TEC and the modified IFM TEC values.

$$R = \frac{TEC_{GAIM}}{TEC_{modIFM}} \tag{10}$$

It was calculated globally and locally, within the region of interest. The calculation was done in MATLAB®, and computed for each 15 min interval, for the corresponding GAIM-GM output, .NC files. The values of the depletion metric, can vary from 0 to very large positive numbers. However, an ideal value will be considered, 1, when the GAIM-GM TEC value is equal to the modified IFM TEC value. The ratio metric gives a multiplicative factor, that describes whether GAIM-GM's output TEC values are either greater than the TEC values on the modified IFM grid ($R > 1$), or less than the TEC values on the modified IFM grid ($R < 1$). This metric is computed at each grid point to analyze spatially GAIM-GM's performance. After the spatial analysis was conducted a temporal evaluation was conducted where the average value of the metric will be computed, defined by Equation 11, and examined over the 96-hour forecast window.

$$R_{mean} = \frac{\sum R}{N} \tag{11}$$

The value of N for each feature is shown in Table 3, showing that the number of points within each feature increases with feature size, which may cause some smoothing in the R_{mean} temporal traces.

Table 3. Number of latitudinal and longitudinal grid points contained in the depleted region, for both the IFM and GAIM grids

Feature #	GAIM Grid Points
1	2
2	8
3	24
4	40
5	60
Global	1056

The difference metric described next will further help aid in determining GAIM-GM's capability to replicate the scintillation feature.

3.7.2.2 Difference Metric: δ

The difference metric is defined in Equation 12. It is referred to as the difference metric because it compares the difference of the GAIM-GM TEC and the background IFM TEC to the difference of the modified IFM TEC and the background IFM TEC.

$$\delta = \frac{TEC_{bkndIFM} - TEC_{GAIM}}{TEC_{bkndIFM} - TEC_{modIFM}} \tag{12}$$

The difference metric determines the extent to which GAIM-GM alters the TEC values within the scintillation feature only. An ideal value for this metric is still 1, where that indicates the GAIM-GM TEC output, has replicated the TEC values within the scintillation feature on the modified IFM grid. In the cases considered here, the scintillation feature is a region of reduced density relative to the background IFM. Thus the denominator will always be positive for all cases. GAIM-GM should try to replicate the feature and therefore produce a TEC value less than the TEC of the IFM background and therefore yielding a positive numerator also. δ values less than 1, indicate the GAIM-GM TEC was not reduced to the TEC values observed in the scintillation region. A δ value greater than 1 indicate GAIM-GM produced

TEC values less than the TEC values observed in the scintillation region. Negative δ values are possible, indicating that GAIM-GM produces TEC values greater than the background IFM. It is important to emphasize, that this metric can only be calculated within the feature, otherwise an infinite value will be obtained. The next section will discuss how these metrics will be utilized to assess GAIM-GM's performance globally and locally.

3.7.3 Evaluation Types

Two different types of analysis were performed on the GAIM-GM TEC output for each constellation and feature combination - global with the feature ingested, and locally, only within the region of interest when the path between the ground station and satellite intercepted the feature. The details of each of these analyses is provided below.

3.7.3.1 Global Evaluation

The global output of GAIM-GM was analyzed to assess GAIM-GM's ability to sense, through satellite ingested data, the presence of artificial scintillation features. The ingested data contains information when the associated scintillation feature is intercepted by the path between the satellite and ground station, and when the path is outside the scintillation feature, sensing the original IFM electron density grid. Here the depletion metric, as defined in Equation 10 and Equation 11 will be used to compute the global metric, where N is the total number of grid points across the globe, listed in Table 3. The goal of this analysis is to determine if ingesting data from a perturbation, in a known location, affects the output of GAIM-GM globally.

3.7.3.2 Local Evaluation

A concern exists that the global analysis may be on too broad of a scale to determine if GAIM-GM was successful in replicating the feature overlaid on the IFM electron density grid. This local analysis measured GAIM-GM's output only for all times throughout the forecast window, for only the grid points within the scintillation feature. Points throughout the forecast window when the slant TEC data ingested pertaining to that particular 15 minute interval, was calculated along a path that fully intercepted the scintillation feature were examined and designated by a dot on the temporal evaluation curves. A diagram showing how the interception condition was determined is shown in Figure 13.

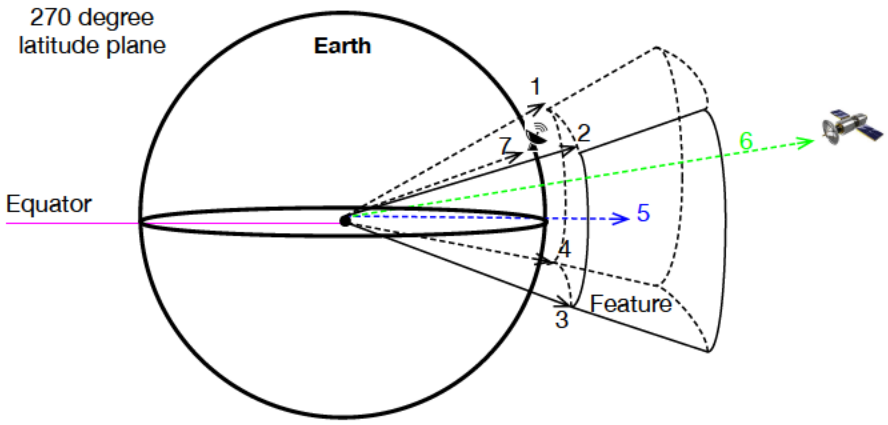

Figure 13. Ground station and satellite line of sight and feature intercept geometry.

The perspective in Figure 13 is such that the plane on the sheet of paper, is the 270 degree meridian. Solid lines indicate features that are within that plane. Dashed

lines indicate features that are into the page. For each feature created, the vectors 1-4 were calculated to the 4 points on base of the feature, from the center of the Earth. Vector 5 is a vector pointing from the center of the Earth to the middle of the depleted region. The angles were calculated between vectors 1 through 4 and vector 5. Vector 6 is the vector from the center of the Earth to the satellite. Next, vector 7 is the vector that points from the center of the earth to the ground station. If that vector falls within the angles calculated between vectors 1 through 4, then it was determined that the ground station was within the local area of the feature. For each ground station that was within the local area of the feature, the STK® access data was examined, containing the ephemeris information of the satellite. If the angle from the vector drawn from the center of the Earth, to the satellite's position obtained from the ephemeris data, vector 6, and vector 5, was within the four angles formed between vectors 1 through 4 and vector 5, the time is recorded. Once all the times were recorded, the times were used to generate the appropriate time format for that particular output file associated with that time. Then all of the .NC files were searched to find, the particular files that contain the appropriate times. This process guaranteed that the entire depth of the feature is captured in the slant TEC calculation, and the depletion and difference metric were only computed when that occurred. For the evaluation types discussed, surface plots of the metrics were made across the GAIM-GM grid, for each satellite constellation and feature combination to examine the spatial variation in the metrics. Additionally, temporal plots were created with the mean ratio metric values plotted for each satellite and feature combination. This allowed for trends in feature size and the number of satellites to be identified.

IV. Analysis and Results

4.1 Chapter Overview

This chapter presents the results from the ratio and the difference metric analysis. The chapter starts off with the global analysis results, looking at the ratio metric mapped over the entire globe. Then the local analysis results are presented, looking at the grid points that lie within the scintillation feature.

4.2 Global Spatial Analysis, Ratio Metric

Global maps containing the values of the ratio metric, R, are presented in Figures 14 and 15 for both day and nighttime, respectively, with variable color bars for contrast to the background.

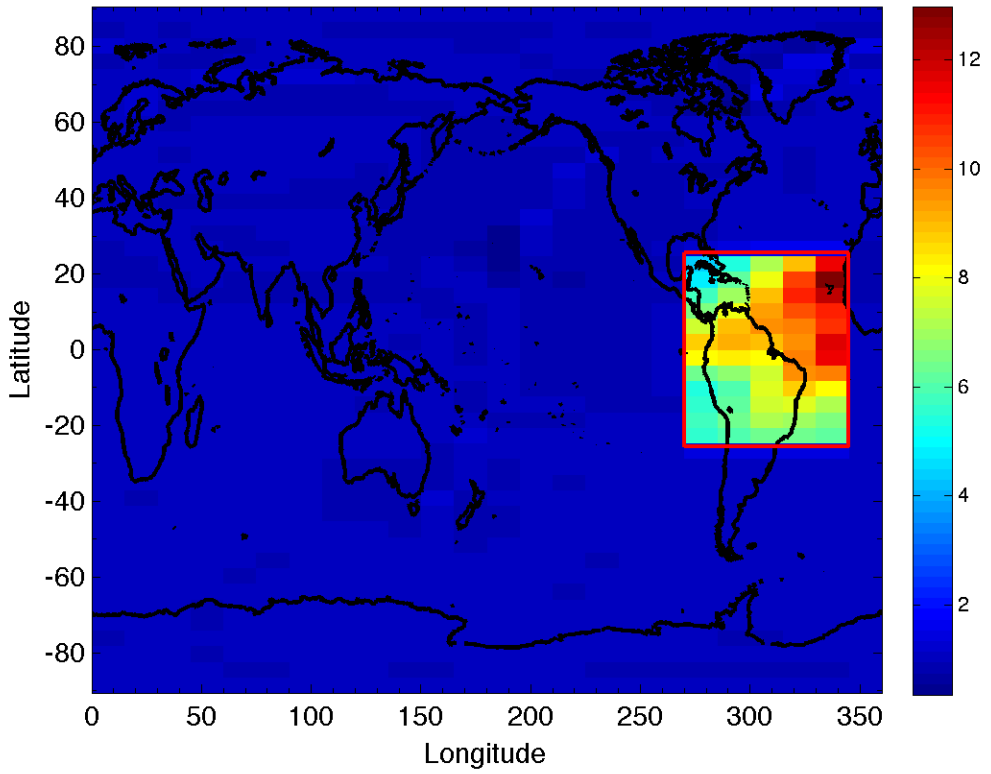

Figure 14. Global ratio metric (unitless) valid at 003/1800Z, daytime within Feature 5, outlined by the red box. Data from 9 satellites were ingested.

During the daytime Figure 14 shows the values vary from 6 through 12 within the feature with R values remaining fairly close to 1 outside of the feature. Outside of the scintillation feature the modified IFM grid mimics the background IFM. When data is assimilated pertaining to the background IFM grid outside of the scintillation region, a value of 1 indicates GAIM-GM replicates the background IFM. This result is what would be expected, and indicates GAIM-GM's data assimilation is working well. When examining the values of R at night, the same trend outside the feature is seen in Figure 15.

Areas outside the scintillation feature in Figure 15 result in near ideal values for R, further indicating GAIM-GM is assimilating the data well when ingesting data outside of the scintillation region. With ideal values outside of the scintillation region,

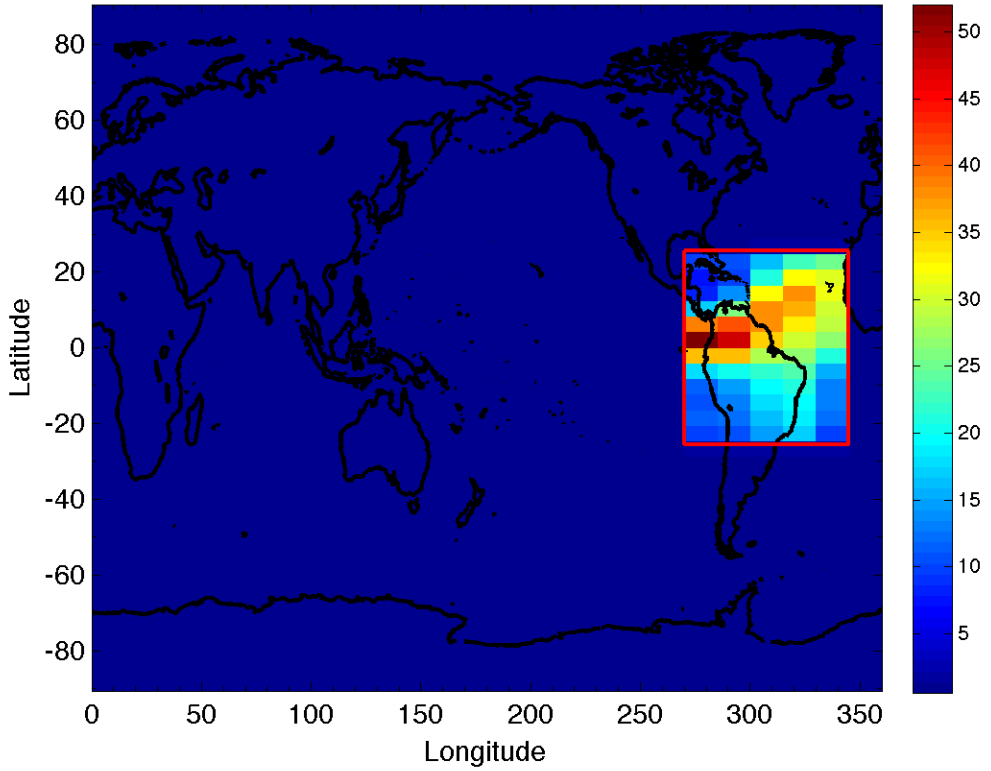

Figure 15. Global ratio metric (unitless) valid at 003/0600Z, nighttime Feature 5, outlined by the red box. Data from 9 satellites were ingested.

performing further analysis on a global scale is not necessary since the metrics only vary within the scintillation region. To investigate this, the R metric for the same time frames are presented zoomed into the local area of the scintillation feature in the next sections.

4.3 Local Spatial Analysis, Ratio Metric

This section is divided into two parts. The first is a discussion of the ratio metric during the daytime. The following section discusses the ratio metric during the nighttime. Figures 16 and 19 will be referenced heavily throughout this section, comparing the behavior of the ratio metric in both day and night.

The first and last rows of pixels in the images may have extreme values presented in the images. This is due to the borders of the figures being drawn based on the

original feature size, which was snapped to the IFM grid. The metrics and TEC images are shown on the GAIM-GM grid, and the extreme values are a result of the nearest neighbor interpolation scheme used to map the IFM grid to the GAIM-GM grid. These values were discarded when computing mean values and investigating the behavior of the metrics, as they gave erroneous or singular results when the mean metric values were computed.

4.3.1 Daytime

A map of the ratio metric R is presented for the grid points within Feature 5 in Figure 16 to closely examine the ratio metric during the day.

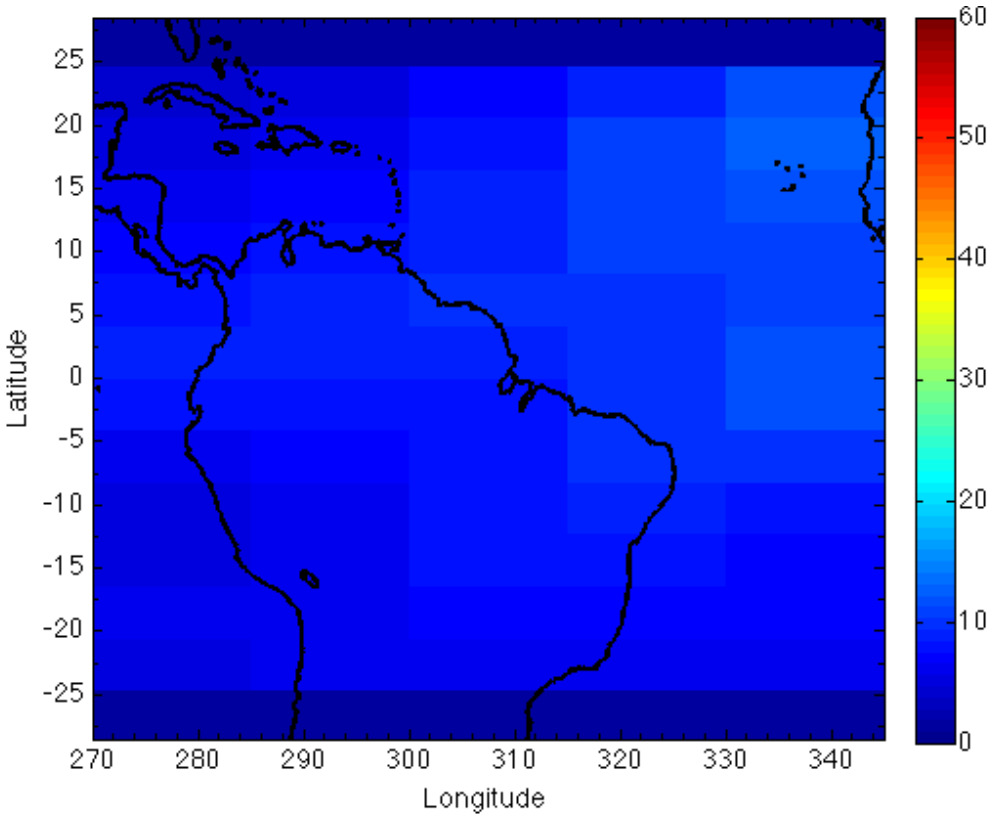

Figure 16. Local ratio metric (unitless) valid at 003/1800Z, daytime within Feature 5. Data from 9 satellites were ingested.

Inside the scintillation feature shown in Figure 16 values of R approach 12, indi-

cating that TEC values in the GAIM-GM output are 12 times larger than the TEC values on the truth ionosphere, or the modified IFM grid. Due to the large vertical extent of the feature, the modified TEC values within the feature were dropped to values varying from approximately 2 to 3, shown in Figure 17 (verified with cursor tool in MATLAB®).

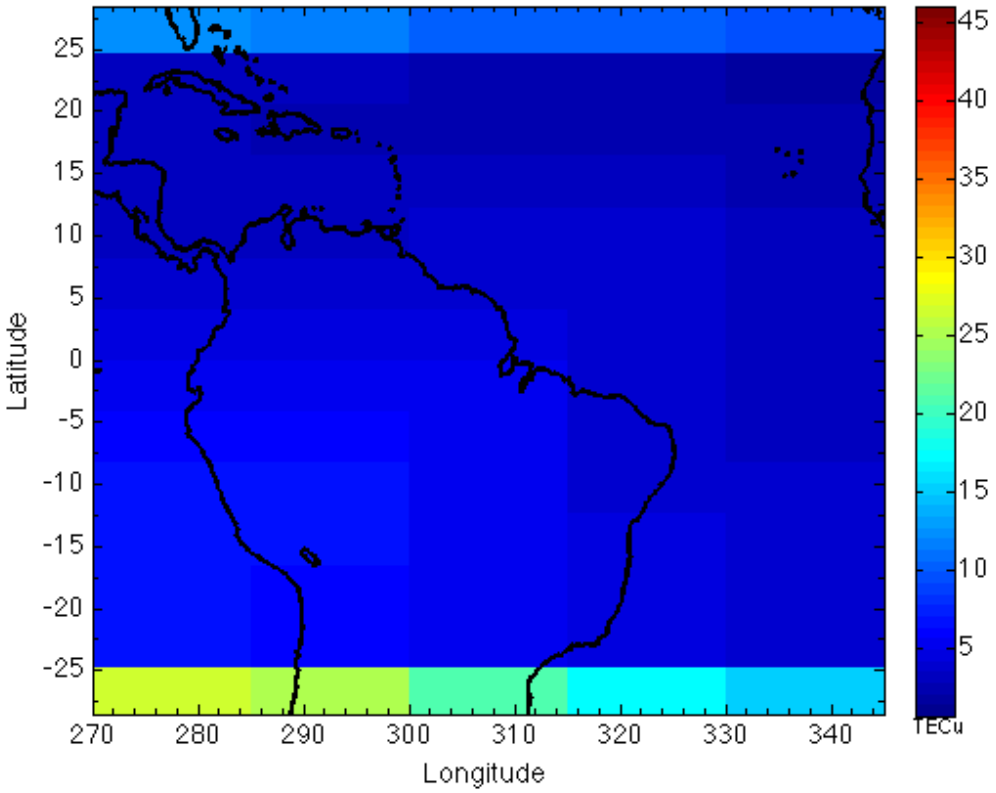

Figure 17. Modified IFM TEC values, valid at 003/1800Z, daytime, within Feature 5.

Although the result within the feature is far from the ideal value of 1, GAIM-GM is still altering the TEC values within the feature. Modified TEC values of 2 to 3 with R values near 12, results in a GAIM-GM TEC value of 36 TECu. With a large swath of TEC values greater than 45 TECu shown in the background IFM, shown in Figure 18, indicating GAIM-GM depleted the TEC value by about 9 TECu, within the scintillation feature.

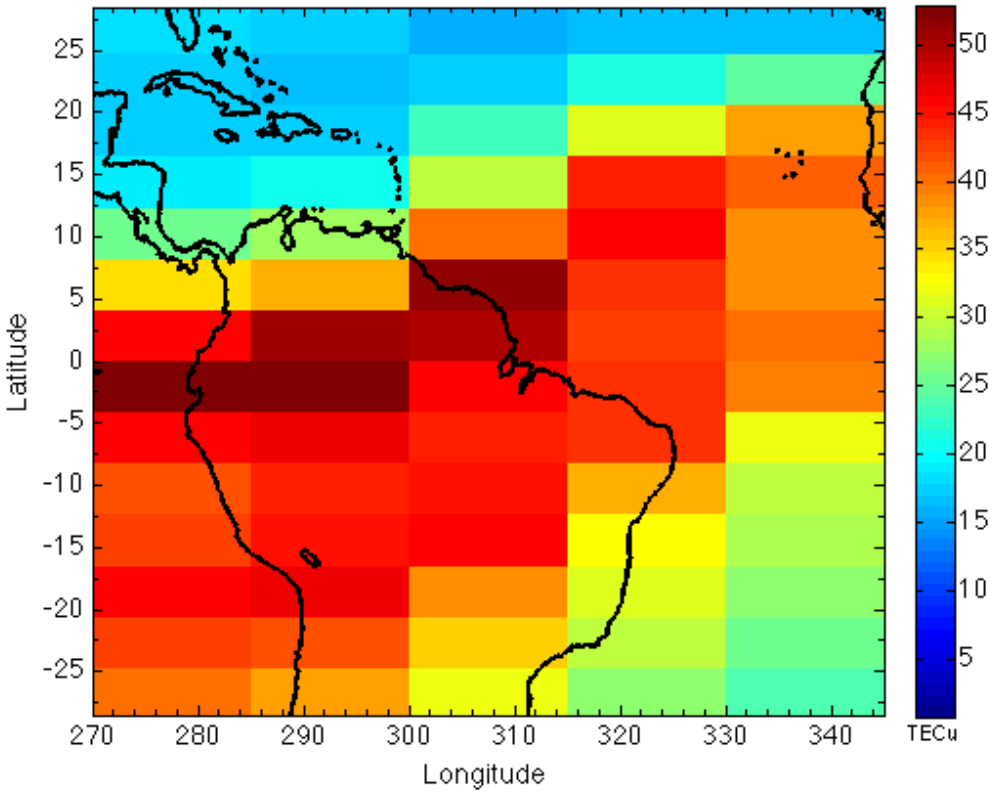

Figure 18. Background IFM TEC values, valid at 003/1800Z, daytime, within Feature 5.

This shows that during the day, for the grid points within the scintillation feature, GAIM-GM is depleting the TEC values but not completely to the modified TEC values, due to the non-ideal values of R. The next section will examine the behavior of R at night.

4.3.2 Nighttime

Another map of the ratio metric within Feature 5 is shown in Figure 19, displaying the values at night.

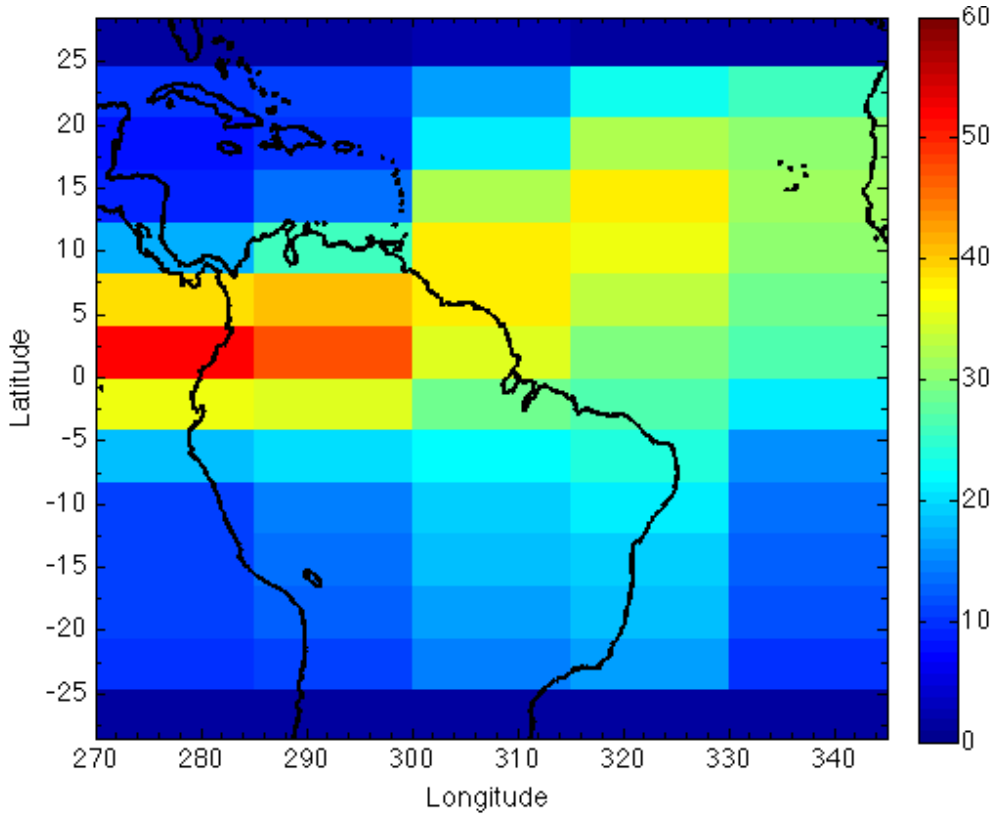

Figure 19. Local ratio metric (unitless) valid at 003/0600Z, nighttime within Feature 5. Data from 9 satellites were ingested.

Values are seen above 50 on the western edge of the feature, with a large swath of values greater than 40 across South America. These large values are due to the feature remaining the same size throughout the forecast window. This results in the same grid points on the IFM electron density grid being zeroed out during the day and the night. At night, the photoionization diminishes, which in turn drives the TEC values of the ionosphere down. Comparing the nighttime background IFM TEC values in Figure 20 to the daytime background IFM TEC values in Figure 18 in the previous section, diminished TEC values are observed during the nighttime.

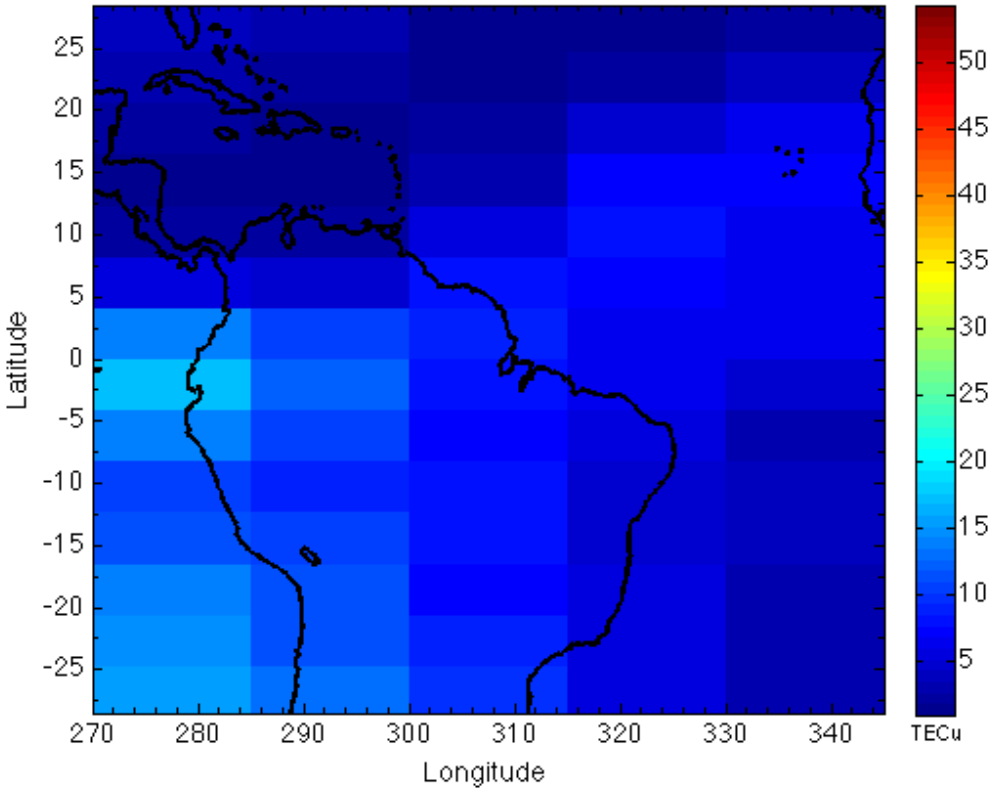

Figure 20. Background IFM TEC values, valid at 003/0600Z, nighttime, within Feature 5

Further eliminating a large portion of the electron density in this nighttime profile will further diminish the TEC values on the modified IFM grid, as shown in Figure 21.

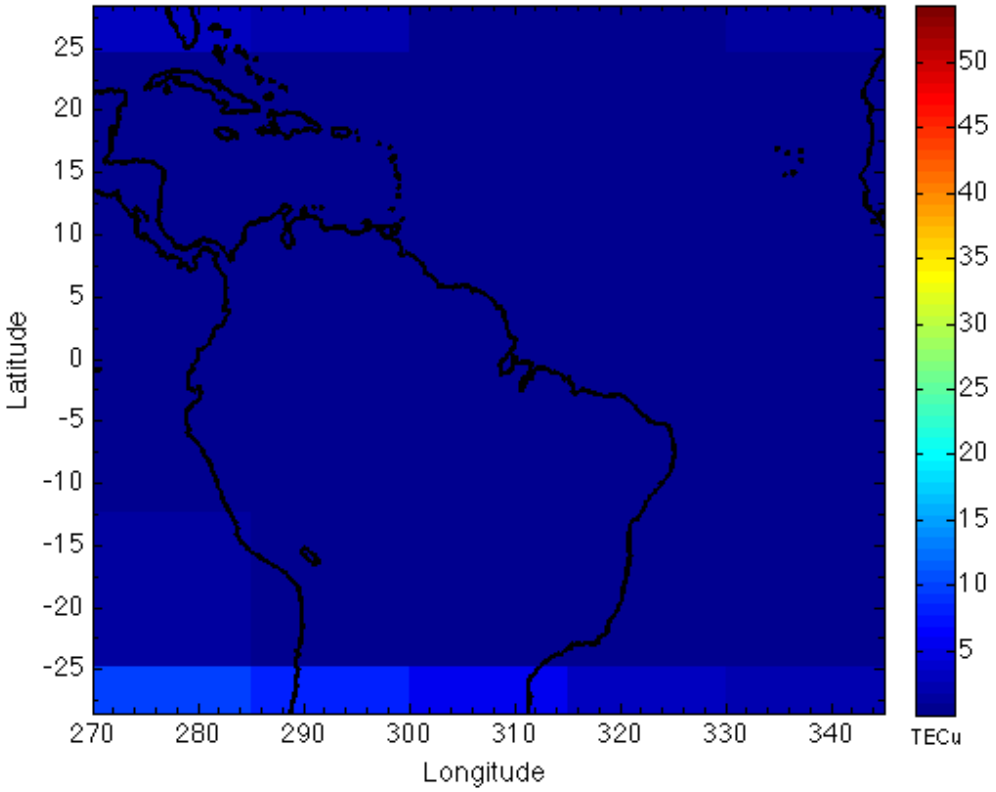

Figure 21. Modified IFM TEC values valid at 003/0600Z, nighttime, within Feature 5

These lowered TEC values, approximately .2 TECu, will result in dividing by a small number in the ratio metric R. As a result, this will drive the values of R upwards at night. With an R value near 55 as shown in Figure 19, yields a GAIM-GM TEC value near 11 TECu. Regions with the large R values, had TEC values near 15 TECu on the background IFM. This indicates that when GAIM-GM ingested data pertaining to the scintillation feature at night, the TEC values were depleted by about 4 TECu, yielding a similar result to what was seen during the day.

The discussion up to this point has dealt only with the largest feature and the 9 satellite constellation. With a good understanding of how the ratio metric will behave diurnally, large values at night and smaller values during the day, temporal plots are provided in the next section to identify trends in feature size and the number

of satellites in the constellation.

4.4 Local Temporal Analysis, Ratio Metric

In order to provide a temporal plot, the average of the values of R was computed for each 15 minute output file. Plots are generated for the 5 different features containing traces for each of the 5 different satellite constellations throughout the forecast window, as shown in Figure 22.

It is seen in Figure 22 that the smallest feature, Feature 1, has the smallest amplitude in diurnal variation with values varying from 1 to 2. Feature 5, the biggest feature, has the largest amplitude in diurnal variation, with values varying from approximately 5 to 30. This is a direct result of the smallest feature having the smallest vertical extent, only 104 km versus 504 km, of electron density zeroed out, yielding modified TEC values close to the background IFM TEC values. This results in the ratio metric remaining close to 1, while the larger features have a larger vertical extent of zero electron density, allowing for the modified TEC values to be smaller, driving the R_{mean} value up at night.

4.5 Ratio Metric Conclusions

The large R_{mean} values at night are seen throughout the entirety of the forecast window, with the peaks falling between sunset and sunrise, indicated by the light and dark dashed lines, respectively. With values during the day never becoming the ideal value, it can be concluded that GAIM-GM performs the data assimilation well, but does not deplete the TEC values within the scintillation feature appropriately.

Another conclusion that can be drawn from Figure 22 is that increasing the feature size and number of satellites in the constellation, the number output files containing ingested information about the scintillation increases. A dot on the curve for each

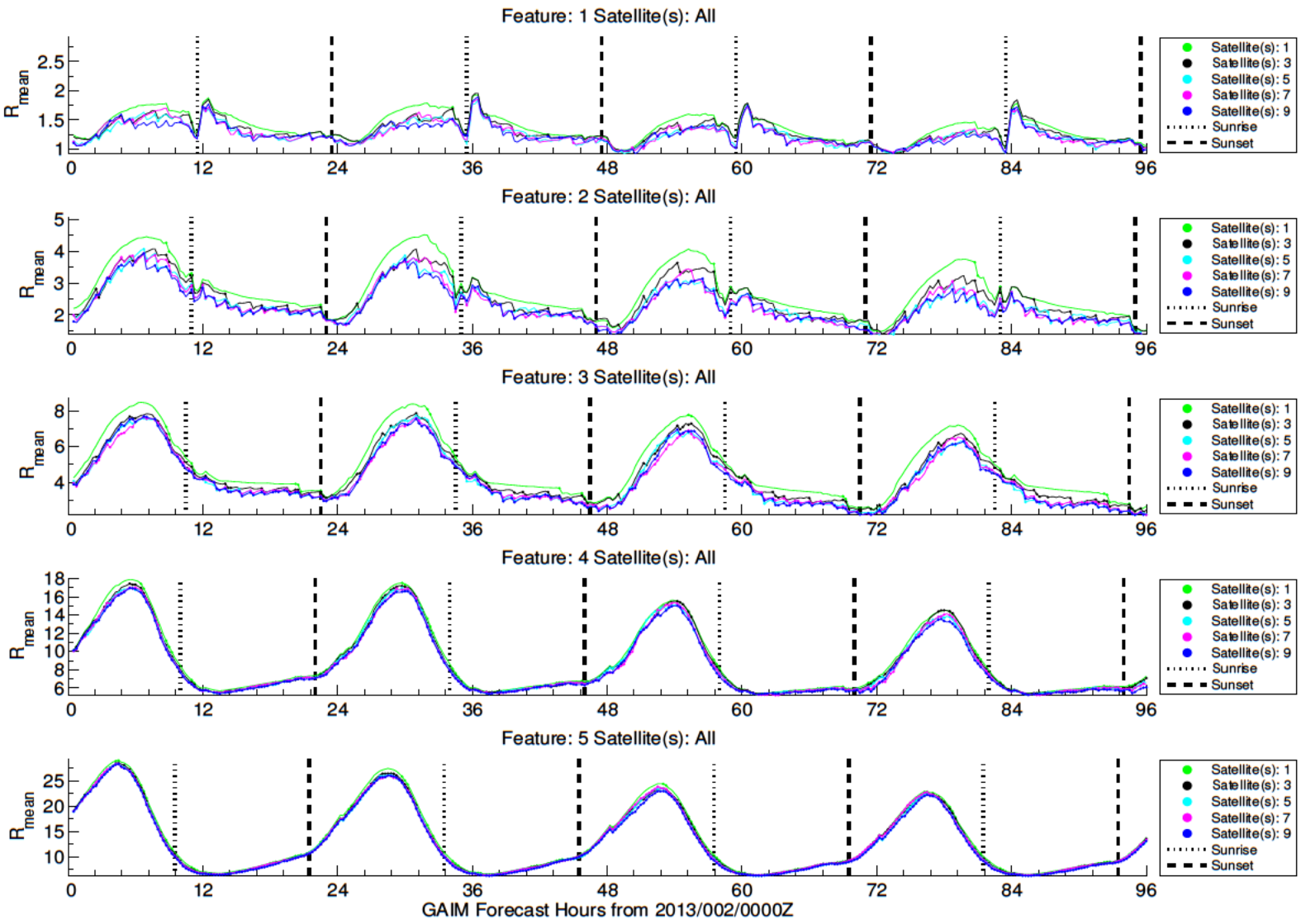

Figure 22. Mean ratio metric evaluated over the entire forecast window, for each feature with data for all of the satellite constellations plotted.

satellite constellation represents an output file that ingested data from the scintillation feature for that particular 15 minute forecast window. This is more explicitly shown in Table 4, where the number of output files containing ingested data for the feature is shown for each combination.

Table 4. Number of output files containing ingested data from the scintillation feature, for the 4 day forecast window.

Feature #	# of Satellites				
	1	3	5	7	9
1	5	15	34	46	64
2	18	55	97	132	167
3	38	115	184	222	231
4	62	181	262	290	296
5	83	253	322	366	371

It is seen increasing the feature size (down the rows) and increasing the number of satellites in the constellation (across the columns) results in a larger amount of output files containing information regarding the scintillation feature. Additionally, across the forecast window, it is seen that increasing the feature size, provides less noise, or variability across individual output files, for R_{mean}. This is due to the R values being averaged over a larger number of grid points for increasing feature size. Finally, with the traces of each satellite constellation plotted for each feature in Figure 22, it is seen that increasing the number of satellites in the constellation does not improve the value of the ratio metric. This comes as a surprise, since increasing the number of satellites increased the amount of data ingested pertaining to the scintillation feature as indicated on Table 4. With the analysis on the ratio metric complete, a quick overview of the difference metric, δ, is provided next.

4.6 Local Spatial Analysis, Difference Metric

Maps of the day and night values of the difference metric are provided in Figures 23 and 24.

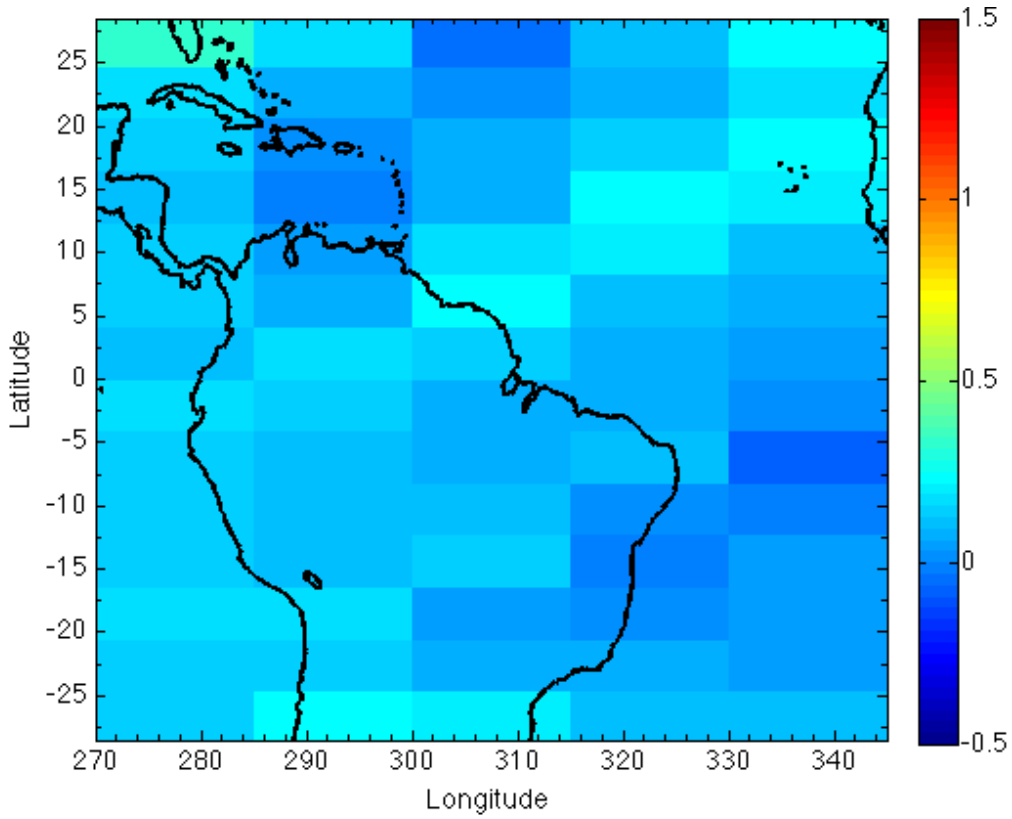

Figure 23. Difference metric for feature 5, valid at 003/1800Z, daytime locally within the feature, for those grid points within the feature only.

The color bars in Figures 23 and 24, are fixed to be able to examine differences in the day and night values. It is seen that at night (Figure 24) values are small, near .05, for the difference metric, with slightly larger values throughout the feature, approximately .2 during the day (Figure 23). This implies that at night GAIM-GM depleted the TEC values by only 5 percent, relative to the background IFM, of what the true scintillation feature contained, and 20 percent accordingly during the daytime. This further shows that the data assimilation performed by GAIM-GM is not depleting the TEC values within the feature completely, to allow GAIM-GM to

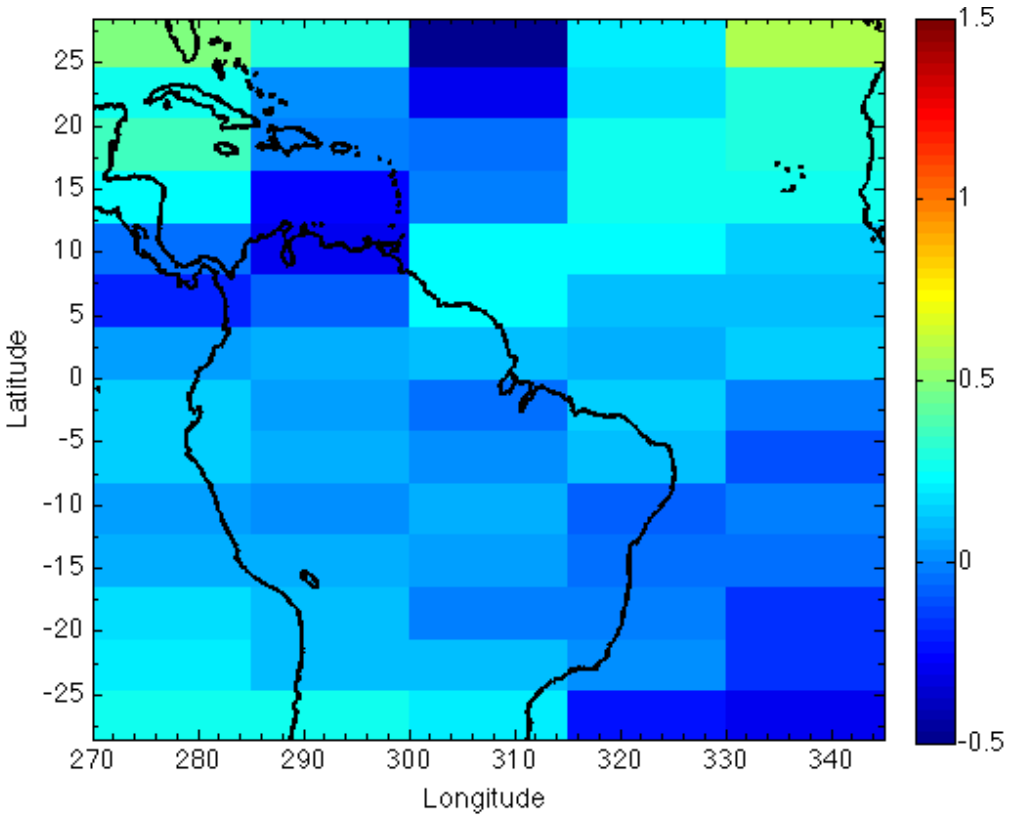

Figure 24. Difference metric for feature 5, valid at 003/0600Z, nighttime locally within the feature, for those grid points within the feature only.

replicate the scintillation feature completely. A summary of the results presented is provided in the last section of this chapter.

4.7 Results Summary

In summary, the results of this analysis indicate that the GAIM-GM data assimilation scheme is working well when ingesting data outside of the scintillation feature. Within the scintillation feature, GAIM-GM does not deplete the TEC values within the scintillation feature enough to truly replicate the feature. It was also shown that increasing the number of satellites in the satellite constellation does not increase the performance of GAIM-GM, however, this result may be due to the limiting the number of orbital planes in the study, providing inadequate coverage of the entire Earth.

The final chapter of this document will recap the work completed and the results obtained, along with provide a framework for future work to be completed.

V. Discussion

5.1 Chapter Overview

This chapter summarizes the work completed in regards to this thesis, and provides conclusions found using the ratio and difference metric. Lastly, this chapter lays the ground work for future work, with GAIM-GM and its sensitivity to scintillation features in the ionosphere.

5.2 Summary

The objectives of this research were completed successfully. Simulated satellite observations were obtained via slant TEC measurements, from a perturbed ionosphere that was characterized by modified IFM output. Those simulated observations were then ingested into the GAIM-GM model, and the output of GAIM-GM was evaluated using two simple metrics.

In collaboration with faculty at Utah State University, model IFM data was obtained. Five different perturbations or features were overlaid on the electron density output. Additionally, five different Walker satellite constellations, were developed in STK®, and numerical slant TEC values were obtained when flying each of these constellations, over the different modified IFM electron density grids. The numerical slant TEC values were obtained by using a method provided by Nava [9]. The calculation was verified using real world TOPEX data, where observed slant TEC values from the study were compared against slant TEC calculations from model IFM data. These slant TEC values were ingested into GAIM-GM, and GAIM-GM's output was examined to see how well GAIM-GM sensed and reproduced the feature.

Once the GAIM-GM output was obtained, four different interpolation schemes were examined. Of the four interpolation schemes the nearest neighbor interpolation

scheme mapping the IFM TEC values to the GAIM-GM grid yielded the best result. Two metrics, ratio and difference metrics, were then developed to help determine GAIM-GM's capability to replicate the features. The ratio metric was calculated on a global scale. It was seen in regions outside of where the feature was introduced the value of the ratio metric did not change. It was determined then to only utilize the metrics for the grid points within the feature.

5.3 Conclusions

When the ratio metric was examined across the globe for each feature and constellation combination, it was seen outside of the feature the metric yielded values close to one. This indicated that when data was assimilated outside of the feature, GAIM-GM handled the data assimilation very well. When the ratio metric was examined inside the latitudinal and longitudinal boundaries of the feature, the ratio metric showed a strong diurnal dependence. Increasing the feature size, forced the modified TEC values to approach zero at night, driving the values of the ratio metric upward. Ratio metric values varied from 2 to 30 at night, for the smallest and largest features, respectively. During the daytime, the magnitude of the metric variation across the features decreased, with values varying from 1.5 to 7 for the smallest and largest features. With the ideal value being one for the ratio metric, values nearly an order of magnitude greater than the ideal value, the ratio metric indicated GAIM-GM is not capable of replicating the depleted TEC values within the scintillation feature completely.

With non-ideal values as a result of examining the ratio metric, the difference metric portrayed how much GAIM-GM actually depleted the TEC values in the latitudinal and longitudinal boundaries of the feature. The difference metric did not show a large diurnal dependence, with values near .2 (GAIM-GM TEC only depleted

20 percent) at night, and .4 during the day. These values indicate that GAIM-GM does not fully deplete the TEC values when data is assimilated containing information of the feature.

There are numerous reasons that play a factor into the limited performance of the GAIM-GM model. The model was run in its standard operational mode, that is currently utilized by the Air Force Weather Agency. There is an option where GAIM-GM can be run in a research mode, where parameters within the model can be adjusted to better account for irregularities in the ingested data. This research did not utilize the research mode in order to be directly applicable to the users of the GAIM-GM model. Another reason is the satellite constellations and ground station network were not optimized. This means that the feature was not always seen throughout the entirety of the forecast window, essentially allowing GAIM-GM to forget the feature existed, and needed to account for the feature again, when it was sensed later in the forecast period. The ground station network also limited the amount of ground stations available to ingest data that would contain information about the feature. If the simulations would have been run on an ideal ground station grid, where the ground station was simulated to be at each latitude and longitude grid point in GAIM-GM, the results might have shown that GAIM-GM can more effectively deplete the TEC values.

5.4 Future Work

The features used in this research were non-physical on a large spatial scale, to account for the lower resolution in the GAIM-GM model. In future work, it is recommended to include physical features observed in the Earth's ionosphere, on a refined resolution. It is anticipated that a finer grid resolution will allow for the smaller, physical feature to be sensed and replicated in the GAIM output.

It was recently discovered that a new version of GAIM will be coming available for operation use within the next year [4]. This version is called GAIM-Full Physics (GAIM-FP). This model uses a different full physics model as the background state in the Kalman filter, called the Ionospheric Plasma Model (IPM). In addition to including an updated model, the way the error covariances are treated in the Kalman filter have been adjusted [4]. Future work could include performing a similar analysis conducted here, ingesting the data into the GAIM-FP model and see how the results differ.

Taking the research one step further, would be to couple the study with the scintillation codes. Here the modified IFM electron density or TEC grids could be used to identify areas of scintillation, and see how the features caused the scintillation codes to react.

GAIM-GM is a very powerful assimilation model, that the Air Force utilizes heavily. Continuing research on the numerical prediction of space weather is extremely important, and will benefit the Air Force greatly.

Appendix A. Ingest File Examples

A.1 Appendix Overview

This appendix provides example data ingest file, for the GAIM-GM runs outlined in Table 2. This appendix starts with an example GPS ingest file, discusses the different properties within the file, and concludes with an example of a satellite ingest file.

A.2 GPS Ingest File Example

This section provides a list of the physical properties needed to build a GPS ingest file, for GAIM-GM input. Table 5 provides a column number, labeled in the header line, in the example file provided in Figure 25. The GPS ingest files for GAIM-GM require the first line to provide header info. For easy reference, column labels were added to allow the reader to interpret what the values represent.

Table 5. GPS ingest file data properties. * indicates an arbitrary value, as not used by GAIM for these simulations.

Column #	Property Descriptor
1	Year
2	Day of the Month
3	Month
4	Hour
5	Minute
6	Second
7	Satellite Number
8	Link*
9	Azimuth Angle
10	Elevation Angle
11	Leveling*
12	Phase TEC
13	Raw Code TEC
14	Code TEC
15	TEC Error*
16	Satellite ECEF X Coordinate
17	Satellite ECEF Y Coordinate
18	Satellite ECEF Z Coordinate
19	Ground Station ECEF X Coordinate
20	Ground Station ECEF Y Coordinate
21	Ground Station ECEF Z Coordinate
22	Phase TEC Error*

Columns 1 through 6 represent date and time information. Column 7 represents the satellite number, where in this research, this value never exceeded 9. Column 8 is what is known as the link number, where since this research was numerical in nature, this number could be any number, so long as it met the format requirements needed. Columns 9 and 10 represent the azimuth and elevation angle computed using the intrinsic MATLAB® functions. The leveling value in column 11 was another arbitrary value that was not needed due to the numerical calculation. In a real world measurement made by a satellite constellation on a ground station grid, three different TEC values would be observed. These would be the phase TEC, raw code TEC, and code TEC indicated in columns 12 through 14. However, in this research the slant TEC value calculated numerically will be used for all 3 of these values. The TEC error in column 15 was held constant, per instruction of the Utah State University faculty. Columns 16 through 18 contain the Earth Centered Earth Fixed (ECEF) Coordinates of the satellite, and 19 through 21 contain the ECEF coordinates of the ground station. Column 22 contains the phase TEC error, which for this research remained constant at 3.85, as directed by Utah State University faculty.

The TEC values ingested for the first 15 minutes are shown in Figure 26. This is an auxiliary output from running the GAIM-GM model at Utah State University, used for testing, where this plot utilizes the information provided by the TEC values calculated, and the elevation and azimuth angles, to computer the vertical TEC above the GPS ground station.

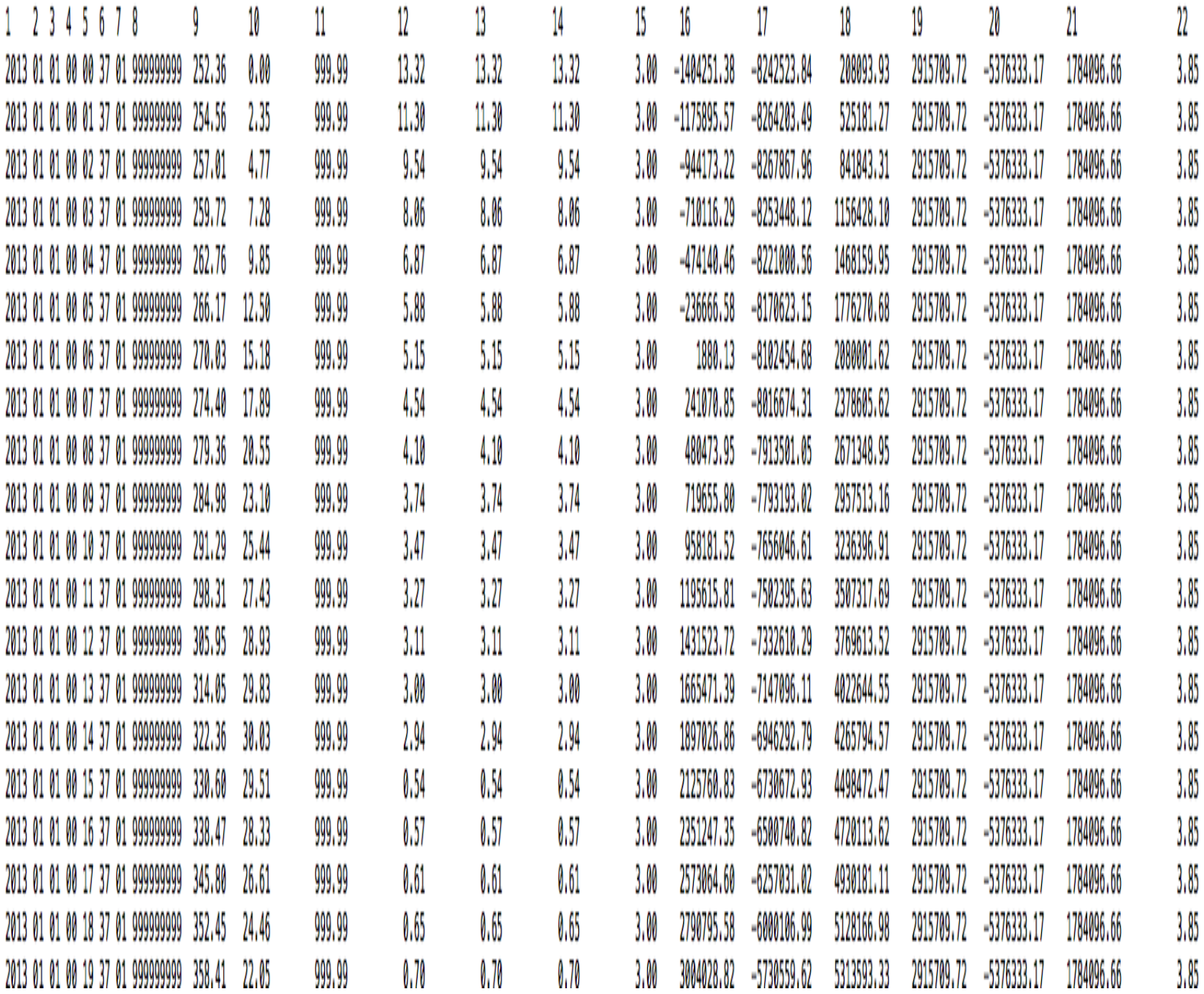

1	2	3	4	5	6	7	8	9	10	11	12	13	14	15	16	17	18	19	20	21	22
2013	01	01	00	00	37	01	9999999999	252.36	0.00	999.99	13.32	13.32	13.32	3.00	-1404251.38	-8242523.84	208093.93	2915709.72	-5376333.17	1784096.66	3.85
2013	01	01	00	01	37	01	9999999999	254.56	2.35	999.99	11.30	11.30	11.30	3.00	-1175895.57	-8264203.49	525181.27	2915709.72	-5376333.17	1784096.66	3.85
2013	01	01	00	02	37	01	9999999999	257.01	4.77	999.99	9.54	9.54	9.54	3.00	-944173.22	-8267867.96	841843.31	2915709.72	-5376333.17	1784096.66	3.85
2013	01	01	00	03	37	01	9999999999	259.72	7.28	999.99	8.06	8.06	8.06	3.00	-710116.29	-8253448.12	1156428.10	2915709.72	-5376333.17	1784096.66	3.85
2013	01	01	00	04	37	01	9999999999	262.76	9.85	999.99	6.87	6.87	6.87	3.00	-474140.46	-8221000.56	1468159.95	2915709.72	-5376333.17	1784096.66	3.85
2013	01	01	00	05	37	01	9999999999	266.17	12.50	999.99	5.88	5.88	5.88	3.00	-236666.58	-8170623.15	1776270.68	2915709.72	-5376333.17	1784096.66	3.85
2013	01	01	00	06	37	01	9999999999	270.03	15.18	999.99	5.15	5.15	5.15	3.00	1800.13	-8102454.68	2080001.62	2915709.72	-5376333.17	1784096.66	3.85
2013	01	01	00	07	37	01	9999999999	274.40	17.89	999.99	4.54	4.54	4.54	3.00	241078.85	-8016674.31	2378605.62	2915709.72	-5376333.17	1784096.66	3.85
2013	01	01	00	08	37	01	9999999999	279.36	20.55	999.99	4.10	4.10	4.10	3.00	480473.95	-7913501.05	2671348.95	2915709.72	-5376333.17	1784096.66	3.85
2013	01	01	00	09	37	01	9999999999	284.98	23.10	999.99	3.74	3.74	3.74	3.00	719655.80	-7793193.02	2957513.16	2915709.72	-5376333.17	1784096.66	3.85
2013	01	01	00	10	37	01	9999999999	291.29	25.44	999.99	3.47	3.47	3.47	3.00	958181.52	-7656046.61	3236396.91	2915709.72	-5376333.17	1784096.66	3.85
2013	01	01	00	11	37	01	9999999999	298.31	27.43	999.99	3.27	3.27	3.27	3.00	1195615.81	-7502395.63	3507317.69	2915709.72	-5376333.17	1784096.66	3.85
2013	01	01	00	12	37	01	9999999999	305.95	28.93	999.99	3.11	3.11	3.11	3.00	1431523.72	-7332618.29	3769613.52	2915709.72	-5376333.17	1784096.66	3.85
2013	01	01	00	13	37	01	9999999999	314.05	29.83	999.99	3.00	3.00	3.00	3.00	1665471.39	-7147096.11	4022644.55	2915709.72	-5376333.17	1784096.66	3.85
2013	01	01	00	14	37	01	9999999999	322.36	30.03	999.99	2.94	2.94	2.94	3.00	1897026.86	-6946292.79	4265794.57	2915709.72	-5376333.17	1784096.66	3.85
2013	01	01	00	15	37	01	9999999999	330.60	29.51	999.99	0.54	0.54	0.54	3.00	2125760.83	-6730672.93	4498472.47	2915709.72	-5376333.17	1784096.66	3.85
2013	01	01	00	16	37	01	9999999999	338.47	28.33	999.99	0.57	0.57	0.57	3.00	2351247.35	-6500740.82	4720113.62	2915709.72	-5376333.17	1784096.66	3.85
2013	01	01	00	17	37	01	9999999999	345.80	26.61	999.99	0.61	0.61	0.61	3.00	2573964.60	-6257031.02	4930181.11	2915709.72	-5376333.17	1784096.66	3.85
2013	01	01	00	18	37	01	9999999999	352.45	24.46	999.99	0.65	0.65	0.65	3.00	2790795.58	-6000106.99	5128166.98	2915709.72	-5376333.17	1784096.66	3.85
2013	01	01	00	19	37	01	9999999999	358.41	22.05	999.99	0.70	0.70	0.70	3.00	3004028.82	-5730559.62	5313593.33	2915709.72	-5376333.17	1784096.66	3.85

Figure 25. Example GPS ingest file, for January 1, 2013, for the ABMF ground station, for hour 00-01Z.

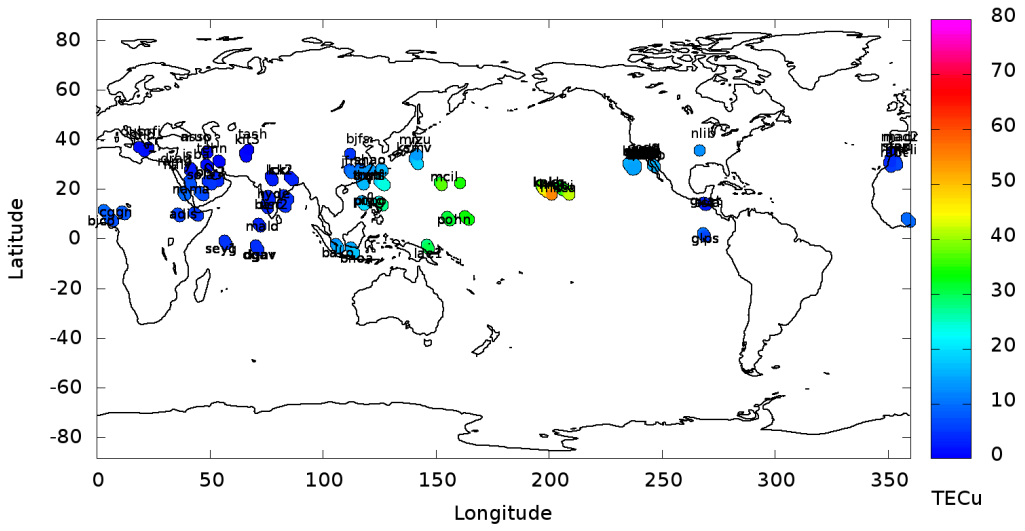

Figure 26. Auxiliary output, showing the ingested GPS TEC values, for Feature 5 and 9 satellite constellation, valid 2013/002/0015Z.

The shaded color corresponds to the TEC value ingested for that particular ground station at that particular location. These types of images are created for every 15 minute interval, for each model run. The next section will outline the properties recorded for the satellite occultation ingest files.

A.3 Satellite Occultation Ingest File Example

This section will discuss the physical properties, listed in Table 6, required to generate the satellite occultation ingest files.

Table 6. Occultation ingest data properties. * indicates an arbitrary value, as not used by GAIM for these simulations.

Column #	Property Descriptor
1	Year
2	Day (Julian Day)
3	Hour
4	Minute
5	Second
6	Satellite Number
7	Satellite Number
8	Link*
9	1st Satellite ECEF X Coordinate
10	1st Satellite ECEF Y Coordinate
11	1st Satellite ECEF Z Coorinate
12	2nd Satellite ECEF X Coordinate
13	2nd Satellite ECEF Y Coordinate
14	2nd Satellite ECEF Z Coordinate
15	Slant TEC
16	Tangent Height
17	Tangent Latitude
18	Tangent Longitude
19	Elevation Angle

The first column in Table 6 matches the property descriptor to the value presented in the appropriate column labeled in Figure 28. First it is important to note, that all occultation ingest files do not require a header line, and the file will not be ingested if

the first line does not contain the data. Column labels were entered manually for easy reference for the reader. Columns 1 through 5 denote date and time information that the slant TEC calculation was made. Columns 6 and 7 denote the satellite number for each satellite used in the calculation. For this research the value in column 6 never exceeded 8 and the value in column 7 never exceeded 9. Column 8 is the link number, where just as in the GPS ingest files, can be any arbitrary number formatted correctly. Columns 9 through 11 denote the ECEF coordinates of the first satellite, while 12 through 14 denote the ECEF coordinates of the second satellite. Column 15 is the slant TEC value along the path between the two satellites. Columns 16 through 18 are the tangent height, latitude and longitude, which denote the 3-D location of the occultation location, projected down to the height of the maximum electron density,

```
function out = tangentCalculation(sat1X, sat1Y, sat1Z, sat2X, sat2Y,
sat2Z)

t0 = .00001;
xd = sat2X-sat1X;
yd = sat2Y-sat1Y;
zd = sat2Z-sat1Z;

tn = 1.5*10^(-2) + t0;
step=1;
while(step==1)
    x = sat1X+xd*tn;
    y = sat1Y+yd*tn;
    z = sat1Z+zd*tn;
    rtan = sqrt(x*x + y*y + z*z);
    h0 = rtan/1000 - 6371;
    if(h0>=300)
        step=0;
    end
    if(tn>1)
        step=0;
    end
    tn = tn+t0;
end

r = sqrt(x*x + y*y + z*z);
theta = atand(y/x);
phi = acosd(z/r);
tan_lat = 90-phi;
tan_lon = mod(360+theta,360);
tan_height = r/1000-6371;
out = [tan_lat tan_lon tan_height];
end
```

Figure 27. Code showing how the tangent latitude, longitude, and altitude are computed.

Column 19 provides the elevation angle, calculated using the intrinsic Matlab

function. In order for these data points to be ingested, the elevation angle from the first satellite to the second satellite needed to be negative. An example of an occultation ingest file (not to scale) is shown in Figure 28.

The data provided in these occultation files is then combined with the GPS ingested data, to provide an overall picture of the locations of the data ingest points into GAIM-GM for each 15 minute window, shown in Figure 29.

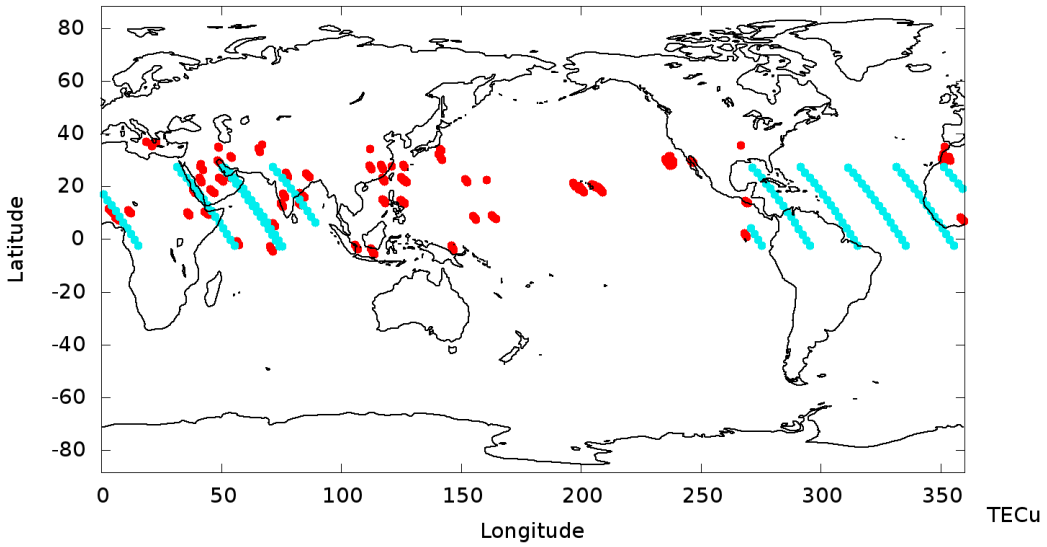

Figure 29. Auxiliary output, showing the ingested satellite occultation land track (teal lines) and ingested GPS sites (red dots), for Feature 5, and 9 satellite constellation, valid 2013/002/0015Z.

The image in Figure 29 is created as an auxiliary output, to provide the model user test information to make sure the model is ingesting the data properly. These images are created for every 15 minute output interval, for each model run.

1	2	3	4	5	6	7	8	9	10	11	12	13	14	15	16	17	18	19
2013	001	00	00	00	01	02	99	-1544533.	-8220006.	10844.	5463664.	-6332656.	6555.	0.000	1946.175	0.1	80.0	-25.7
2013	001	00	01	00	01	02	99	-1317449.	-8252921.	329210.	5631328.	-6175555.	324660.	0.000	1946.275	2.3	81.6	-25.7
2013	001	00	02	00	01	02	99	-1087371.	-8267748.	646764.	5786717.	-6004839.	641964.	0.000	1946.572	4.5	83.2	-25.6
2013	001	00	03	00	01	02	99	-854705.	-8264476.	962722.	5929568.	-5820818.	957684.	0.000	1947.061	6.6	84.8	-25.5
2013	001	00	04	00	01	02	99	-619863.	-8243136.	1276305.	6059649.	-5623835.	1271041.	0.000	1947.739	8.8	86.4	-25.4
2013	001	00	05	00	01	02	99	-383263.	-8203802.	1586739.	6176754.	-5414262.	1581263.	0.000	1948.597	11.0	88.0	-25.2
2013	001	00	06	00	01	02	99	-145327.	-8146586.	1893260.	6280707.	-5192499.	1887585.	0.000	1949.629	13.2	89.7	-25.0
2013	001	00	07	00	01	02	99	93517.	-8071643.	2195113.	6371364.	-4958977.	2189253.	0.000	1950.824	15.3	271.3	-24.8
2013	001	00	00	00	01	07	99	-1544533.	-8220006.	10844.	-7389666.	-3917524.	6968.	0.000	1946.175	0.1	78.7	-25.7
2013	001	00	01	00	01	07	99	-1317449.	-8252921.	329210.	-7274095.	-4115370.	325612.	0.000	1946.275	2.3	80.3	-25.7
2013	001	00	02	00	01	07	99	-1087371.	-8267748.	646764.	-7142513.	-4304276.	643452.	0.000	1946.572	4.5	81.8	-25.6
2013	001	00	03	00	01	07	99	-854705.	-8264476.	962722.	-6995163.	-4483920.	959704.	0.000	1947.061	6.6	83.4	-25.5
2013	001	00	04	00	01	07	99	-619863.	-8243136.	1276305.	-6832328.	-4654000.	1273588.	0.000	1947.739	8.8	85.0	-25.4
2013	001	00	05	00	01	07	99	-383263.	-8203802.	1586739.	-6654322.	-4814234.	1584331.	0.000	1948.598	11.0	86.6	-25.2
2013	001	00	06	00	01	07	99	-145327.	-8146586.	1893260.	-6461498.	-4964364.	1891166.	0.000	1949.629	13.2	88.3	-25.0
2013	001	00	07	00	01	07	99	93517.	-8071643.	2195113.	-6254242.	-5104152.	2193339.	0.000	1950.824	15.3	90.0	-24.8
2013	001	00	00	00	02	03	99	5463664.	-6332656.	6555.	8357611.	323313.	-2671.	0.000	1946.175	0.0	311.5	-25.7
2013	001	00	01	00	02	03	99	5631328.	-6175555.	324660.	8339668.	552432.	315387.	0.000	1946.274	2.2	313.0	-25.7
2013	001	00	02	00	02	03	99	5786717.	-6004839.	641964.	8303426.	780439.	632665.	0.000	1946.570	4.4	314.6	-25.6
2013	001	00	03	00	02	03	99	5929568.	-5820818.	957684.	8248965.	1006935.	948383.	0.000	1947.058	6.6	316.2	-25.5
2013	001	00	04	00	02	03	99	6059649.	-5623835.	1271041.	8176405.	1231526.	1261761.	0.000	1947.734	8.8	317.8	-25.4
2013	001	00	05	00	02	03	99	6176754.	-5414262.	1581263.	8085908.	1453818.	1572026.	0.000	1948.592	11.0	319.4	-25.2
2013	001	00	06	00	02	03	99	6280707.	-5192499.	1887585.	7977678.	1673424.	1878414.	0.000	1949.623	13.1	321.1	-25.0
2013	001	00	07	00	02	03	99	6371364.	-4958977.	2189253.	7851958.	1889962.	2180172.	0.000	1950.816	15.3	322.8	-24.8
2013	001	00	00	00	03	04	99	8357611.	323313.	-2671.	4958106.	6735821.	-9885.	0.000	1946.174	-0.0	2.9	-25.7
2013	001	00	01	00	03	04	99	8339668.	552432.	315387.	4768132.	6864729.	308373.	0.000	1946.272	2.2	4.5	-25.7
2013	001	00	02	00	03	04	99	8303426.	780439.	632665.	4567619.	6978635.	625871.	0.000	1946.566	4.4	6.0	-25.6
2013	001	00	03	00	03	04	99	8248965.	1006935.	948383.	4356925.	7077350.	941823.	0.000	1947.053	6.5	7.6	-25.5
2013	001	00	04	00	03	04	99	8176405.	1231526.	1261761.	4136434.	7160723.	1255452.	0.000	1947.727	8.7	9.2	-25.4
2013	001	00	05	00	03	04	99	8085908.	1453818.	1572026.	3906555.	7228636.	1565984.	0.000	1948.583	10.9	10.9	-25.2
2013	001	00	06	00	03	04	99	7977678.	1673424.	1878414.	3667715.	7281006.	1872654.	0.000	1949.612	13.0	12.5	-25.0
2013	001	00	07	00	03	04	99	7851958.	1889962.	2180172.	3420365.	7317785.	2174708.	0.000	1950.804	15.2	14.2	-24.8
2013	001	00	00	00	04	05	99	4958106.	6735821.	-9885.	-2174954.	8076118.	-9655.	0.000	1946.175	-0.1	54.3	-25.7
2013	001	00	01	00	04	05	99	4768132.	6864729.	308373.	-2393840.	8008046.	308902.	0.000	1946.271	2.1	55.9	-25.7
2013	001	00	02	00	04	05	99	4567619.	6978635.	625871.	-2607568.	7922376.	626696.	0.000	1946.563	4.3	57.5	-25.6
2013	001	00	03	00	04	05	99	4356925.	7077350.	941823.	-2815769.	7819273.	942945.	0.000	1947.049	6.5	59.1	-25.5
2013	001	00	04	00	04	05	99	4136434.	7160723.	1255452.	-3018084.	7698941.	1256866.	0.000	1947.722	8.7	60.7	-25.4
2013	001	00	05	00	04	05	99	3906555.	7228636.	1565984.	-3214168.	7561625.	1567687.	0.000	1948.577	10.8	62.3	-25.2
2013	001	00	06	00	04	05	99	3667715.	7281006.	1872654.	-3403691.	7407608.	1874642.	0.000	1949.606	13.0	63.9	-25.0
2013	001	00	07	00	04	05	99	3420365.	7317785.	2174708.	-3586334.	7237214.	2176975.	0.000	1950.796	15.1	65.6	-24.8
2013	001	00	00	00	05	06	99	-2174954.	8076118.	-9655.	-7670229.	3334934.	-2155.	0.000	1946.175	-0.1	285.7	-25.7
2013	001	00	01	00	05	06	99	-2393840.	8008046.	308902.	-7753135.	3121441.	316573.	0.000	1946.271	2.1	287.3	-25.7
2013	001	00	02	00	05	06	99	-2607568.	7922376.	626696.	-7819066.	2901006.	634521.	0.000	1946.564	4.3	288.9	-25.6
2013	001	00	03	00	05	06	99	-2815769.	7819273.	942945.	-7867922.	2674020.	950902.	0.000	1947.050	6.5	290.5	-25.5
2013	001	00	04	00	05	06	99	-3018084.	7698941.	1256866.	-7899641.	2440890.	1264937.	0.000	1947.724	8.7	292.1	-25.4
2013	001	00	05	00	05	06	99	-3214168.	7561625.	1567687.	-7914199.	2202038.	1575852.	0.000	1948.579	10.9	293.7	-25.2
2013	001	00	06	00	05	06	99	-3403691.	7407608.	1874642.	-7911612.	1957900.	1882880.	0.000	1949.608	13.0	295.4	-25.0
2013	001	00	07	00	05	06	99	-3586334.	7237214.	2176975.	-7891936.	1708925.	2185267.	0.000	1950.800	15.2	297.0	-24.8
2013	001	00	00	00	06	07	99	-7670229.	3334934.	-2155.	-7389666.	-3917524.	6968.	0.000	1946.174	-0.0	337.2	-25.7
2013	001	00	01	00	06	07	99	-7753135.	3121441.	316573.	-7274095.	-4115370.	325612.	0.000	1946.273	2.2	338.7	-25.7
2013	001	00	02	00	06	07	99	-7819066.	2901006.	634521.	-7142513.	-4304276.	643452.	0.000	1946.567	4.4	340.3	-25.6
2013	001	00	03	00	06	07	99	-7867922.	2674020.	950902.	-6995163.	-4483920.	959704.	0.000	1947.054	6.6	341.9	-25.5
2013	001	00	04	00	06	07	99	-7899641.	2440890.	1264937.	-6832328.	-4654000.	1273588.	0.000	1947.730	8.7	343.5	-25.4
2013	001	00	05	00	06	07	99	-7914199.	2202038.	1575852.	-6654322.	-4814234.	1584331.	0.000	1948.587	10.9	345.1	-25.2
2013	001	00	06	00	06	07	99	-7911612.	1957900.	1882880.	-6461498.	-4964364.	1891166.	0.000	1949.617	13.1	346.8	-25.0
2013	001	00	07	00	06	07	99	-7891936.	1708925.	2185267.	-6254242.	-5104152.	2193339.	0.000	1950.811	15.2	348.5	-24.8

Figure 28. Example satellite occultation ingest file for January 1, 2013, valid 0007.30-0022.30Z.

Bibliography

1. Space Environment Corporation. Ionospheric Forecast Model Version 4.4a, 2002.

2. Kenneth Fenton. *Assessment of the Effects of Plasma Bubbles on GAIM-GM*. Masters, Air Force Institute of Technology, 2011.

3. Lee-Lueng Fu, Edward J Christensen, Charles A. Yamarone, Michael Lefebvre, Yves Menard, Michel Dorrer, and Philippe Escudier. TOPEX/POSEIDON mission overview. *Journal of Geophysical Research*, 99(C12):24,369–24,381, 1994.

4. Larry Gardner. Research Scientist, Center for Atmospheric and Space Sciences, Utah State University, Logan UT. Personal Communication., 2014.

5. International GNSS Service. http://igscb.jpl.nasa.gov/network/network.php, 2014.

6. K. M. Groves, E. J. Weber, M. Smitham, H. Kuenzler, C. E. Valladares, R. Sheehan, E. MacKenzie, J. A. Secan, P. Ning, W. J. McNeill, D. W. Moonan, and M. J. Kendra. Equatorial scintillation and systems support. *Radio Science*, 32(5):2047–2064, 1997.

7. Bruce M. Howe, Kay Runciman, and James Secan. Tomography of the Ionosphere: Four-dimensional simulations. *Radio Science*, 33(1):109–128, 1998.

8. Michael C. Kelley. *The Earth's Ionosphere: Plasma Physics and Electrodynamics*. Academic Press, Inc., 1989.

9. Omar A Nava. *Analysis of Plasma Bubble Signatures in the Ionosphere*. Masters, Air Force Institute of Technology, 2011.

10. Gerd W. Prolss. *Physics of the Earth's Space Environment*. Springer, New York, 2004.

11. L Scherliess, R W Schunk, J J Sojka, and D C Thompson. Development of a physics-based reduced state Kalman filter for the ionosphere. *Radio Science*, 39:1–12, 2004.

12. L Scherliess, R W Schunk, J J Sojka, D C Thompson, and L Zhu. Utah State University Global Assimilation of Ionospheric Measurements Gauss-Markov Kalman filter model of the ionosphere : Model description and validation. *Journal of Geophysical Research*, 111(A11315), 2006.

13. Robert Schunk and Andrew Nagy. *Ionospheres: Physics, Plasma Physics, and Chemistry*. Cambridge University Press, 2009.

14. Robert W. Schunk, Sojka J J, and J V Eccles. Expanded Capabilities for the Ionospheric Forecast Model. Technical report, Air Force Research Laboratory, 1997.

15. Robert W. Schunk, Ludger Scherliess, Jan J. Sojka, Donald C. Thompson, David N. Anderson, Mihail Codrescu, Cliff Minter, Timothy J. Fuller-Rowell, Roderick a. Heelis, Marc Hairston, and Bruce M. Howe. Global Assimilation of Ionospheric Measurements (GAIM). *Radio Science*, 39(1), February 2004.

16. D C Ã Thompson, L Scherliess, J J Sojka, and R W Schunk. The Utah State University Gauss Markov Kalman filter of the ionosphere : The effect of slant TEC and electron density profile data on model fidelity. *Journal of Atmospheric and Solar-Terrestrial Physics*, 68:947–958, 2006.

17. Robert Thompson. Wright Patterson AFB, Personal Communication, 2014.

18. Systems Toolkit User Documentation. http://help.agi.com/resources/help/online/, 2014.

19. L Zhu, R W Schunk, G Jee, L Scherliess, J J Sojka, and D C Thompson. Validation study of the Ionosphere Forecast Model using the TOPEX total electron content measurements. *Radio Science*, 41(RS5S11), 2006.

Vita

Captain Brandon McClung grew up in the great state of Ohio. In October 1994, he moved to Strongsville, OH where he graduated from Strongsville High School, in the top 5 percent of his class, in June 2005. In August 2005, he attended the University of Oklahoma, pursuing a meteorology degree. In May 2009. Captain McClung commissioned as a Second Lieutenant through the ROTC program, in addition to graduating (with honors) from the University of Oklahoma, with a Bachelors of Science degree in Meteorology, 3 minors, in Computer Science, Mathematics, and Aerospace Studies. Additionally, he was accepted into the renowned Honors Society, Phi Beta Kappa.

Captain McClung's first operational assignment was to the 25th Operational Weather Squadron, at Davis Monthan AFB. Here he was certified in all operational floor positions, serving primarily as the Lead Meteorologist and Senior Duty Officer. In November 2011, Capt McClung PCS'd to the 51st Operational Support Squadron, at Osan AB, Korea. Here he was the Wing Weather Officer, and interim Flight Commander. Additionally, Captain McClung was handpicked to serve as the 51st Operational Group Executive Officer. In May 2013 Captain McClung attended the Air Force Institute of Technology, where he received a Masters of Science in Applied Physics, with a concentration in Space Physics. In March 2015, Captain McClung will move to the 2nd Weather Squadron, Air Force Weather Agency, where he will be in command of the Space Weather Operations Center.

REPORT DOCUMENTATION PAGE

Form Approved
OMB No. 0704–0188

1. REPORT DATE (DD–MM–YYYY)	2. REPORT TYPE	3. DATES COVERED *(From — To)*
26-03-2015	Master's Thesis	May 2013 – Mar 2015

4. TITLE AND SUBTITLE
Investigating GAIM-GM's Capability to Sense Ionospheric Irregularities via Walker Satellite Constellations

5a. CONTRACT NUMBER
5b. GRANT NUMBER
5c. PROGRAM ELEMENT NUMBER

6. AUTHOR(S)
McClung, Brandon T, Capt

5d. PROJECT NUMBER
5e. TASK NUMBER
5f. WORK UNIT NUMBER

7. PERFORMING ORGANIZATION NAME(S) AND ADDRESS(ES)
Air Force Institute of Technology
Graduate School of Engineering and Management (AFIT/EN)
2950 Hobson Way
WPAFB OH 45433-7765

8. PERFORMING ORGANIZATION REPORT NUMBER
AFIT-ENP-MS-15-M-076

9. SPONSORING / MONITORING AGENCY NAME(S) AND ADDRESS(ES)
Intentionally Left Blank

10. SPONSOR/MONITOR'S ACRONYM(S)
11. SPONSOR/MONITOR'S REPORT NUMBER(S)

12. DISTRIBUTION / AVAILABILITY STATEMENT
DISTRIBUTION STATEMENT A:
APPROVED FOR PUBLIC RELEASE; DISTRIBUTION UNLIMITED.

13. SUPPLEMENTARY NOTES

14. ABSTRACT

GAIM-GM is a modularized physics based data assimilation model, which ingests data from multiple data sources. One data source is slant total electron content (TEC) from a ground station network to satellites, and along the occultation path between multiple satellites. This study examines GAIM-GM's capability to sense a depleted region in the ionosphere, overlaid on an IFM electron density grid, from satellite constellations ingesting the slant TEC values into GAIM-GM. Satellite constellations were developed in STK®. A real ground station network, generated from IGS, was ingested into STK®, to compute access times to the satellite constellation, and compute slant TEC values on the perturbed IFM grid. The size of the feature was varied along with the number of satellites in the Walker constellation. 25 different scenarios with these parameters varied were created to determine the sensitivity of GAIM-GM to sense the feature. A simple heuristic algorithm was applied comparing the truth data, in this case the perturbed IFM grid, to the GAIM-GM output in each scenario across the entire grid, and for those grid points within the feature.

15. SUBJECT TERMS
Ionosphere, GPS, GAIM, IFM, Satellites

16. SECURITY CLASSIFICATION OF:			17. LIMITATION OF ABSTRACT	18. NUMBER OF PAGES	19a. NAME OF RESPONSIBLE PERSON
a. REPORT	b. ABSTRACT	c. THIS PAGE			Dr. William F. Bailey, AFIT/ENP
U	U	U	U	81	19b. TELEPHONE NUMBER (Include Area Code) (937) 255-3636, x4555; william.bailey@afit.edu